COLO–HEP–395
SLAC-PUB-7796
HEPSY 98-1
April 23, 1998

PENGUIN DECAYS OF B MESONS

Karen Lingel [1]
Stanford Linear Accelerator Center
Stanford University, Stanford, CA 94309

and

Tomasz Skwarnicki [2]
Department of Physics, Syracuse University
Syracuse, NY 13244

and

James G. Smith [3]
Department of Physics, University of Colorado
Boulder, CO 80309

Submitted to *Annual Reviews of Nuclear and Particle Science*

[1]Work supported by Department of Energy contract DE-AC03-76SF00515
[2]Work supported by National Science Foundation contract PHY 9807034
[3]Work supported by Department of Energy contract DE-FG03-95ER40894

PENGUIN DECAYS OF B MESONS

Karen Lingel Stanford Linear Accelerator Center
Tomasz Skwarnicki Department of Physics, Syracuse University
James G. Smith Department of Physics, University of Colorado

KEYWORDS: loop CP-violation charmless

ABSTRACT: Penguin, or loop, decays of B mesons induce effective flavor-changing neutral currents, which are forbidden at tree level in the Standard Model. These decays give special insight into the CKM matrix and are sensitive to non-standard model effects. In this review, we give a historical and theoretical introduction to penguins and a description of the various types of penguin processes: electromagnetic, electroweak, and gluonic. We review the experimental searches for penguin decays, including the measurements of the electromagnetic penguins $b \to s\gamma$ and $B \to K^*\gamma$ and gluonic penguins $B \to K\pi$, $B^+ \to \omega K^+$ and $B \to \eta' K$, and their implications for the Standard Model and New Physics. We conclude by exploring the future prospects for penguin physics.

CONTENTS

1 INTRODUCTION

In the Standard Model, flavor-changing neutral currents (FCNC) are forbidden, for example, there is no direct coupling between the b quark and the s or d quarks. Effective FCNC are induced by one-loop, or "penguin", diagrams, where a quark emits and re-absorbs a W thus changing flavor twice, as in the $b \to t \to s$ transition depicted in Fig. 1. Penguin decays have become increasingly appreciated in recent years. These loop diagrams with their interesting combinations of CKM matrix elements give insight into the Standard Model. In addition, they are quite sensitive to new physics.

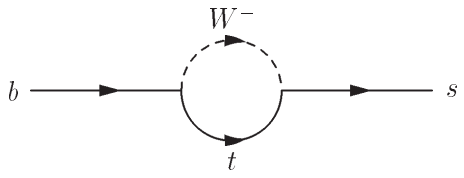

Figure 1: $b \to s$ loop or "penguin" diagram. Of course, in order to conserve energy and momentum, an additional particle is understood to be emitted in the transition.

The weak couplings of the quarks are given by the Cabibbo-Kobayashi-Maskawa (CKM) [1] matrix of complex amplitudes:

$$V_{\rm CKM} = \begin{pmatrix} V_{ud} & V_{us} & V_{ub} \\ V_{cd} & V_{cs} & V_{cb} \\ V_{td} & V_{ts} & V_{tb} \end{pmatrix} \tag{1}$$

For the Standard Model with three generations, the CKM matrix can be described completely by three Euler-type angles, and a complex phase. In the Wolfenstein parameterization [2], the CKM matrix is approximated in terms of four real, independent, parameters, (λ, A, ρ, η), which makes clear the hierarchical structure of the elements:

$$V_{\rm CKM} \approx \begin{pmatrix} 1 - \frac{1}{2}\lambda^2 & \lambda & A\lambda^3(\rho - i\eta) \\ -\lambda & 1 - \frac{1}{2}\lambda^2 & A\lambda^2 \\ A\lambda^3(1 - \rho - i\eta) & -A\lambda^2 & 1 \end{pmatrix} \tag{2}$$

Since $\lambda \equiv \sin\theta_C$, the well-known Cabibbo angle, is small ($\lambda \approx 0.22$), this parameterization shows that the off-diagonal elements are small and the diagonal elements are close to 1. The complex phase, which may be responsible for CP violation in the Standard Model, has been assigned to the corner elements in this parameterization.

1.1 History of Penguins

The curious name penguin goes back to a game of darts in a Geneva pub in the summer of 1977, involving theorists John Ellis, Mary K. Gaillard, Dimitri Nanopoulos and Serge Rudaz (all then at CERN) and experimentalist Melissa Franklin (then a Stanford student, now a Harvard professor). Somehow the telling of a joke about penguins evolved to the resolution that the loser of the dart game would use the word penguin in their next paper. It seems that Rudaz spelled Franklin at some point, beating Ellis (otherwise we might now have a detector named penguin); sure enough the seminal 1977 paper on loop diagrams in B decays [3] refers to such diagrams as penguins. This paper contains a whimsical acknowledgment to Franklin for "useful discussions" [4].

Prior to 1975, the loop diagram had been neglected. Vainshtein, Zakharov, and Shifman [5] discovered the importance of the penguin diagrams, and suggested that penguins were responsible for the enhancement of the $\Delta I = 1/2$ amplitude compared to the $\Delta I = 3/2$ amplitude in weak $K \to \pi\pi$ decays. Penguins were considered in the B system by Ellis, *et al.* [3], and determined to be small compared to $b \to c$ amplitudes. However, Guberina, Peccei, and Rückl [6] later pointed out that the penguin $b \to s$ decays could have a rate as large as tree-level $b \to u$ decays. From Eqn. 2, we see that penguin decays involve $|V_{tb}V_{ts}| \propto \lambda^2$, whereas $b \to u$ transitions involve $|V_{ub}V_{ud}| \propto \lambda^3$. In 1979, the role of penguins in CP violation was pointed out by Bander, Silverman and Soni [7] who showed that interference between penguin diagrams and tree-level diagrams could give large CP asymmetries in B decays. In 1982, Eilam [8] added the gluonic penguin $b \to sg$ to the inclusive penguin rate. Later large QCD corrections to the radiative penguin $b \to s\gamma$ [9] were calculated. These corrections increased the predicted $b \to s\gamma$ rate by a factor of ~ 3, enough to make experimentalists sanguine about measuring the rate. The inclusive gluonic penguin $b \to sg^*$ was later clarified to include the time-like $b \to sq\bar{q}$, and space-like $b\bar{q} \to s\bar{q}$ as well as the light-like $b \to sg$ [10], which increased the gluonic penguin rate [11].

In 1993, the CLEO Collaboration published the first evidence for electromagnetic penguins (Sec. 4.1) in the channel $B \to K^*\gamma$. In 1994 they also measured the inclusive $b \to s\gamma$ rate (Sec. 4.2) which was in good agreement with the theoretical predictions. In 1997, after many hints in several experiments, CLEO found first evidence for gluonic penguin decays (Sec. 5).

1.2 The Importance Of Penguins

Although $s \to u$ loop diagrams are important in K decays, those decays are typically dominated by large non-perturbative effects. A notable exception is $K^+ \to \pi^+\nu\bar{\nu}$ (charge conjugate states are implied throughout this review). This decay is expected to be dominated by electroweak penguins (Sec. 2.2) and could eventually provide a measurement of $|V_{td}|$. Penguin processes are also possible in c and t decays, but these particles have the CKM-favored decays $c \to s$ and $t \to b$ accessible to them. Since the b quark has no kinematically-allowed CKM-favored decay (Eqn. 2), the relative importance of the penguin decay is greater. The mass of the top quark, the main contributor to the loop, is large, and the coupling of the b quark to the t quark, $|V_{tb}|$, is very close to unity, both strengthening the effect of the penguin. The $b \to s$ ($b \to d$) penguin transition is sensitive to $|V_{ts}|$ ($|V_{td}|$) which will be extraordinarily difficult to measure in top decay. Information from

the penguin decay will complement information on $|V_{ts}|$ and $|V_{td}|$ from B_s–$\bar{B}_s$ and B^0–$\bar{B}^0$ mixing.

Since the Standard Model (SM) loops involve the heaviest known particles (t, W, Z), rates for these processes are very sensitive to non-SM extensions with heavy charged Higgs or supersymmetric particles. Therefore, measurements of loop processes constitute the most sensitive low energy probes for such extensions to the Standard Model.

2 THEORY

In sections 2.1 through 2.5 we give general descriptions of various kinds of penguins. Details of the effective Hamiltonian theory are given in section 2.6. Sections 2.7 and 2.8 discuss two important topics in penguin decay: CP Violation and New Physics.

2.1 Electromagnetic Penguins

In electromagnetic penguin decays such as $b \to s\gamma$, a charged particle emits an external real photon (Fig. 2). The hard photon emitted in these decays is an excellent experimental signature. The inclusive rate is dominated by short distance (perturbative) interactions and can be reliably predicted. QCD corrections enhance the rate and have been calculated precisely. Assuming unitarity of the CKM matrix to constrain $|V_{ts}|$ the Standard Model predicts [12] $\mathcal{B}(b \to s\gamma) = (3.5 \pm 0.3) \times 10^{-4}$. Unfortunately, uncertainties in the hadronization process limit the ability to predict individual exclusive rates from first principles of the theory. Phenomenological predictions range from 1% to 40% [16] for the ratio $R_{K^*} \equiv \mathcal{B}(B \to K^*\gamma)/\mathcal{B}(b \to s\gamma)$.

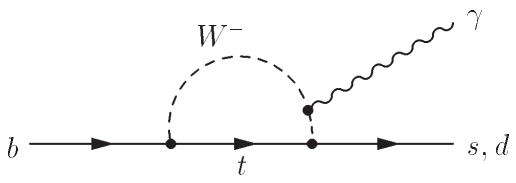

Figure 2: Feynman diagram for the electromagnetic penguins $b \to s\gamma$ and $b \to d\gamma$. The photon can be emitted from the W (shown) or from any of the quarks.

The electromagnetic penguin decay $b \to d\gamma$ is further suppressed by $|V_{td}|^2/|V_{ts}|^2$ and gives an alternative to B^0–$\bar{B}^0$ mixing for extracting $|V_{td}|$. Experimentally, inclusive $b \to d\gamma$ has large backgrounds from the dominant $b \to s\gamma$ decays which must be rejected using good particle identification or kinematic separation.

2.2 Electroweak Penguins

The decay $b \to s\ell^+\ell^-$ can proceed via an electroweak penguin diagram where an emitted virtual photon or Z^0 produces a pair of leptons (Fig. 3a,b). This decay can also proceed via a box diagram (Fig. 3c). The SM prediction for the $b \to s\ell^+\ell^-$ decay rate is two orders of magnitude smaller than the $b \to s\gamma$ rate [13, 20].

The rate for $b \to s\nu\bar{\nu}$ is enhanced relative to $b \to s\ell^+\ell^-$ primarily due to summing the three neutrino flavors. These decays are expected to be dominated by the weak penguin, since neutrinos do not couple to photons. The predicted rate is only a factor of 10 lower than for $b \to s\gamma$ [21]. Unfortunately, the neutrinos escape detection, making this decay mode difficult to observe.

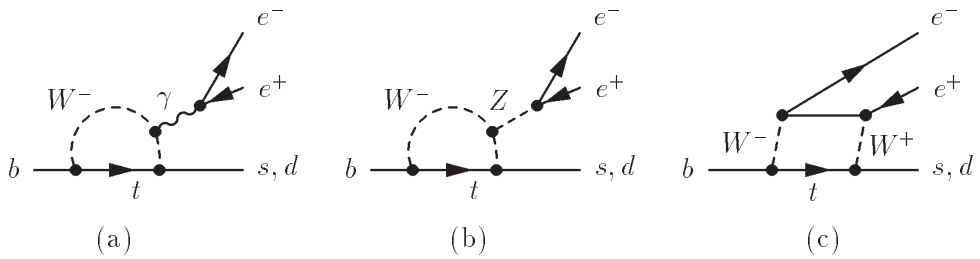

Figure 3: (a) Photon penguin (b) Z^0 penguin and (c) box diagrams for the electroweak decay $b \to (s,d)\ell^+\ell^-$. The diagrams for $b \to (s,d)\nu\bar{\nu}$ are similar, except that (a) does not contribute.

2.3 Vertical Electroweak Penguins

Another category of penguin is the so-called vertical or annihilation penguin where the penguin loop connects the two quarks in the B meson (Fig. 4). These rates are expected to be highly suppressed in the Standard Model since they involve a $b \to d$ transition and are suppressed by $(f_B/m_B)^2 \approx 2 \times 10^{-3}$, where f_B is the B-meson decay constant which parameterizes the probability that the two quarks in the B meson will "find each other", and m_B is the B meson mass. The $B \to \gamma\gamma$ decay is suppressed relative to $b \to s\gamma$ by an additional α_{QED}. The $B \to \ell^+\ell^-$ decays are helicity-suppressed. Because these decays are so suppressed in the Standard Model, they provide a good opportunity to look for non-SM effects (Sec. 2.8).

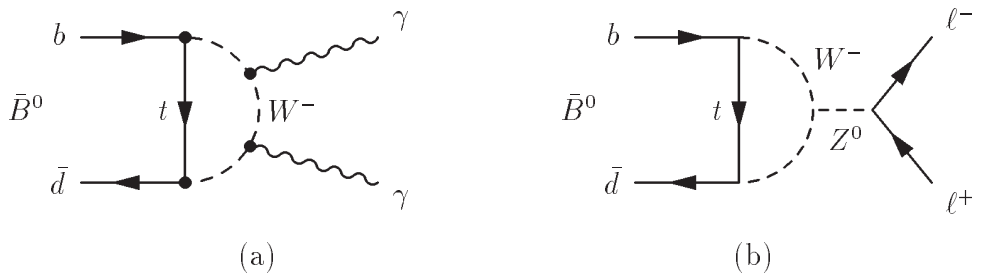

Figure 4: Vertical or annihilation penguins: (a) $B \to \gamma\gamma$ and (b) $B \to \ell^+\ell^-$.

2.4 Gluonic Penguins

An on- or off-shell gluon can also be emitted from the penguin loop. (Fig. 5). While the on-shell $b \to sg$ rate had been calculated to be $\mathcal{O}(0.1\%)$, the inclusive

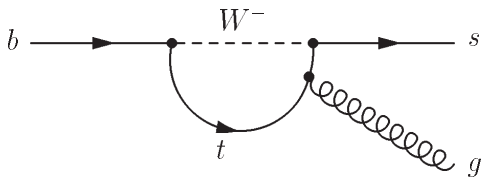

Figure 5: Feynman diagram for the gluonic penguin $b \to sg^*$. The gluon can be emitted from any of the quark lines and can be on-shell or off-shell.

on- plus off-shell $b \to sg^*$ rate includes contributions from $b \to sq\bar{q}$ and $b \to sgg$ which increase the inclusive rate to 0.5–1% [10, 11]. The $b \to dg^*$ penguin rate is smaller by $|V_{td}/V_{ts}|^2$. Unfortunately, there are several difficulties associated with gluonic penguins. There is no good signature for the inclusive $b \to sg^*$ decay, unlike the $b \to s\gamma$ case. The branching fraction of individual exclusive gluonic penguin channels is typically quite small and hadronization effects are difficult to calculate. In addition, many gluonic penguin final states are accessible via other diagrams (Sec. 2.5) so the gluonic penguin is difficult to assess. Thus the "smoking-gun" penguin processes such as $B^0 \to \phi K^0$ that have contributions only from gluonic penguins are eagerly sought.

2.5 Other Contributions to Hadronic Final States

While the gluonic penguin gives rise only to hadronic final states, several other processes can contribute to the same final states. One important contribution is from the tree-level $b \to u$ decay. For example, the $b \to u\bar{u}s$ transition (Fig. 6a) and the $b \to sg^*$ penguin transition both contribute to $B^0 \to K^+\pi^-$. However, the $b \to u\bar{u}s$ transition is Cabibbo-suppressed, so the penguin process is expected to dominate. On the other hand, in $B \to \pi^+\pi^-$ for example, the small $b \to dg^*$ contribution is expected to be dominated by the non-Cabibbo-suppressed tree-level $b \to u\bar{u}d$ transition. In general, most decays to hadronic final states with ϕ mesons or non-zero net strangeness are expected to be dominated by gluonic penguins and hadronic final states with zero net strangeness are expected to be dominated by tree-level $b \to u$.

Electroweak penguins also contribute to hadronic final states. Every gluonic penguin diagram can be converted to an electroweak penguin by replacing the gluon with a Z^0 or γ (Fig. 6b). Electroweak penguins with internal Z^0 or γ emission are suppressed relative to the corresponding strong gluonic penguin. In the hairpin process (Fig. 6c) the gluon, Z^0, or γ is emitted externally and subsequently forms a meson (similar to the leptonic electroweak penguins in Figs. 3a and b). External gluon emission is OZI-suppressed [22]: the color-octet gluon has difficulties forming a color-singlet meson! These hairpin processes, such as $B \to \phi\pi$, are expected to be dominated by electroweak penguins. A possible exception involves decays such as $B \to \eta' K$, where it has been suggested that a gluonic-hairpin diagram could be significant (Sec. 5.1.3).

The vertical electroweak penguin diagram, similar to Fig. 4b, with the lepton pair replaced by a di-quark pair, is highly suppressed and is important only for decays such as $B^0 \to \phi\phi$, where no other diagrams contribute.

In the annihilation diagram the b and $\bar{u}$ quarks in a B^- meson annihilate to form a virtual W^-. The annihilation diagram is suppressed by $|V_{ub}|$ and by

f_B/m_B and is expected to be mostly negligible. In the exchange diagram, a $b \to u$ transition and a $\bar{d} \to \bar{u}$ transition occur simultaneously via the exchange of a W between the b and $\bar{d}$ quarks in a $\bar{B}^0$ meson. The exchange process is also suppressed by $|V_{ub}|$ and f_B/m_B, and is also expected to be negligible, except in decays such as $B^0 \to K^+K^-$ where no favored diagrams contribute.

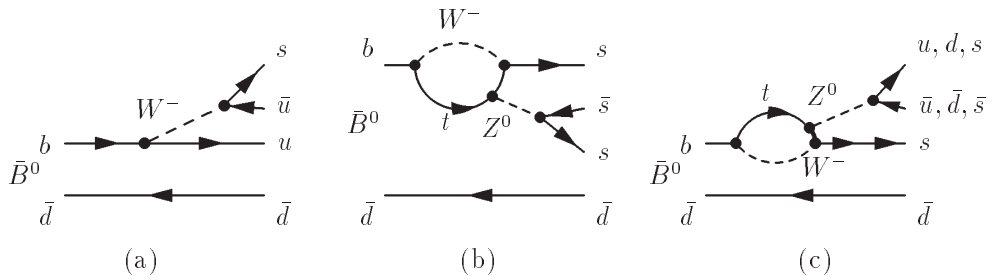

Figure 6: Examples of other diagrams which contribute to hadronic final states: (a) tree-level Cabibbo-suppressed $b \to u\bar{u}s$, (b) electroweak penguin (c) hairpin diagram.

2.6 Effective Theory of Penguin Decays

At high energy scales, $\mu \sim M_W \sim 80$ GeV, quark decays are governed by Feynman diagrams such as those depicted in the previous sections. To obtain an effective low energy theory relevant for scales $\mu \sim m_b \sim 5$ GeV, heavy degrees of freedom must be integrated out to obtain an effective coupling for point-like interactions of initial and final state particles [23]. For semileptonic decays (e.g. the familiar $\beta-$decays in nuclear physics), this integration corresponds to derivation of the Fermi theory of point-like four-fermion interactions from Electroweak Quantum Field Theory. The effective theory relevant for penguin decays is obtained by generalization of the Fermi theory, as depicted in Fig. 7. The heavy degrees of freedom in loop decays are W, Z^0 and t. After the integration they don't appear explicitly in the theory, but their effects are hidden in the effective gauge coupling constants, running masses and, most importantly, in the so-called Wilson coefficients (C_i) describing the effective strength of the local operators (Q_i) generated by electroweak and strong interactions. The operators can be grouped into three categories: $i = 1, 2$ — current-current operators (Fig. 6a); $i = 3, \ldots, 6$ — gluonic penguin operators (related to diagrams in Fig. 5); $i = 7, \ldots, 10$ — electro-weak penguin operators (Figs. 2 and 3). The effective Hamiltonian for $b \to s$ penguin decays has the following form:

$$\mathcal{H}_{\rm eff} = -\frac{4\,G_F}{\sqrt{2}}\,V_{tb}V_{ts}^*\sum_{i=1}^{10} C_i(\mu)\,Q_i(\mu)$$

Technically, the calculations are performed at a high energy scale $\mu \sim M_W$, and then evolved to a low energy scale $\mu \sim m_b$ using renormalization group equations. This evolution mixes the operators: $C_i(\mu) = \sum_j U_{ij}(\mu, M_W)C_j(M_W)$. The renormalization guarantees that the μ dependence of C_i is canceled by the μ dependence of Q_i, thus any observable quantity should not depend on the renormalization scale μ. However, since the calculations are performed perturbatively,

the truncation of the perturbative series induces μ dependence of the theoretical predictions, which often dominates the theoretical uncertainty. Higher order terms must be included to minimize the μ dependence.

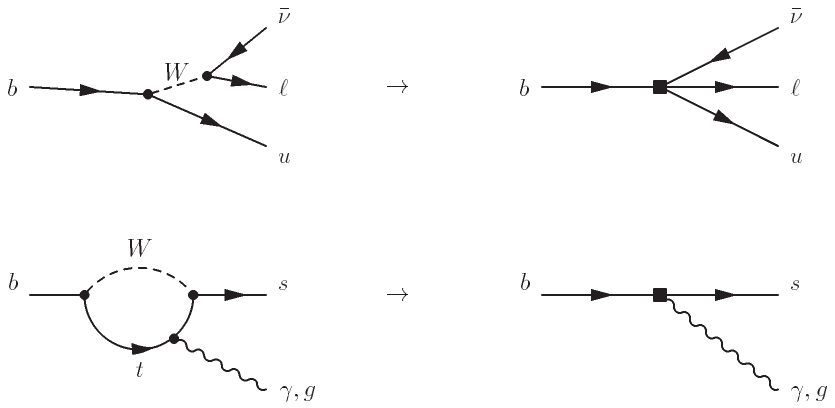

Figure 7: Derivation of effective low energy theory from high energy Quantum Field Theory. Derivation of the Fermi theory of the W exchange diagram for semileptonic $b \to u\, l \nu$ decay ("$\beta-$decay") is shown at the top. Generalization for the loop processes $b \to s\, \gamma$ and $b \to s\, g$ are shown at the bottom [24].

Even though renormalization mixes the operators, specific processes are mostly sensitive to a small subset of Wilson coefficients. For example: $b \to s\, \gamma$ to C_7, $b \to s\, l^+ l^-$ to C_7, C_9 and C_{10}.

Since extensions of the Standard Model contribute additional diagrams at the high energy scale, they modify the values of the Wilson coefficients in the effective low energy theory.

While Wilson coefficients represent short distance (i.e. high energy) electroweak and strong interactions, the operator elements $< X|Q_i|B >$ are influenced by long distance (i.e. low energy) strong interactions (here $|B>$ represents the B meson and $|X>$ its decay mode). Therefore, unlike the Wilson coefficients, the operator elements cannot be obtained perturbatively due to the confining nature of strong interactions at large distances.

Fortunately, when $|X>$ represents an inclusive final state, expansion in powers of $1/m_b$ shows that to leading order $< X|Q_i|B > \approx < s|Q_i|b >$, where $< s|Q_i|b >$ is an operator element for free quarks which can be easily calculated. The first non-perturbative corrections are of second order [25], $\mathcal{O}(1/{m_b}^2)$, and are small, thanks to the heavy b quark mass. Experimentalists must sum over all possible hadronic final states to determine an inclusive rate. For example, $\mathcal{B}(B \to X_s\, \gamma) \approx \mathcal{B}(b \to s\, \gamma)$, where X_s represents a collection of charmless hadrons with net strangeness -1.

When $|X>$ is an exclusive final state it is difficult to obtain $< X|Q_i|B >$ from first principles. Numerical treatment of strong quantum fields (Lattice QCD) has been useful so far only for the simplest cases in which part of the final state is non-hadronic, $|X>=|h\, L>$, such as $B \to K^* \gamma$. Since leptons and photons are not involved in long distance interactions, the operator element factorizes into hadronic and non-hadronic currents, $< h\, L|Q_i|B >=< h|J_1|B >< L|J_2|0 >$. The latter can be written explicitly. Non-leptonic final states are the most difficult

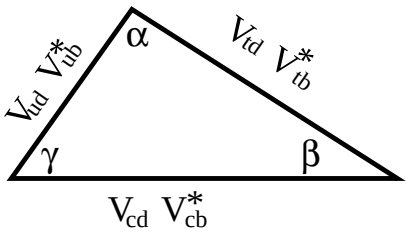

Figure 8: The Unitarity Triangle.

to calculate. Heavy Quark Effective Theory, which is so useful for describing ordinary $b \to c$ decays, is of little use for $b \to s, d$ decays, since the final state quarks are light. Phenomenological models used to predict rates for gluonic penguin decays make many assumptions, the accuracy of which is often difficult to assess, and the scope of the predictions is usually limited to two-body final states. The approach which has often been employed [26, 27, 28] is based on factorization [29]. The rationale of factorization in hadronic decays lies in the phenomenon of color-transparency [30], in which one expects intuitively that a pair of fast-moving quarks (in two-body decays $E_h \sim m_B/2$) in a color-singlet state effectively decouples from soft gluons. Therefore, long distance final state interactions (FSI) can be neglected. Short distance FSI mediated by hard gluon exchanges can be included perturbatively. The latter are important for predictions of the strong phases which make direct CP violation possible. With the factorization ansatz, the matrix elements $< h_1 h_2 | Q_i | B >$ can be expressed as a product of two hadronic currents: $< h_1 | J_1 | B >< h_2 | J_2 | 0 >$. This involves both the matrix elements of the singlet-singlet and octet-octet currents J_i. Since the octet-octet matrix elements are not directly measured they are usually discarded. To compensate for this, the effective strengths of the singlet-singlet current matrix elements are renormalized by replacing the inverse of the number of colors ($1/N_c$) by a phenomenological color parameter ξ. While the assumption of factorization works well for tree-level $b \to c$ decays [31, 32], its applicability to penguin and $b \to u$ decays needs to be verified. Also it is not clear if a single parameter ξ will suffice to incorporate non-perturbative effects in all ten operators of the effective Hamiltonian.

2.7 CP Violation

Unitarity of the CKM matrix (Eqn. 1) leads to several constraints, the most interesting of which is the orthogonality of the first and third columns:

$$V_{ud} V_{ub}^* + V_{cd} V_{cb}^* + V_{td} V_{tb}^* = 0 \tag{3}$$

Eqn. 3 defines a triangle in the complex plane (Fig. 8) called the Unitarity Triangle. The lengths of the sides of the Unitarity Triangle are given by the magnitudes of the CKM matrix elements. The angles are given by the phase of the CKM matrix elements: β is the phase of V_{ub}, γ is the phase of V_{td}, and $\alpha \equiv \pi - \beta - \gamma$. Physicists wish to measure the sides of the triangle, and independently measure the angles in order to check the consistency of the Standard Model.

The CPT theorem forbids partial rate asymmetries which are CP violating to occur at tree level. The addition of the penguin diagram, with different CKM matrix elements and thus different weak phases, allows quantum interference between two amplitudes, and therefore can produce direct CP violation. CP

violation caused by interference between the penguin and tree processes can lead, for instance, to rate asymmetries in B^+ *vs.* B^- decays. There are also schemes to measure γ or α using relations between tree-level and penguin amplitudes and isospin relations in $B \to K\pi$ and related decays [33]. Many of the most promising measurements of CP violation in the B system rely on interference caused by B^0–$\bar{B}^0$ mixing (indirect CP violation). For example, the penguin decays $B^0 \to \phi K_S^0$ and $B^0 \to \eta' K_S^0$ can be used to measure β [35, 36]. The tree-dominated decay $B^0 \to \pi^+\pi^-$ can be used to measure α; however, additional penguin diagrams can cause direct CP violation as well as indirect, which may complicate extraction of α. This effect is known as penguin pollution.

2.8 Non-Standard Model Possibilities

Penguin diagrams are a very good place to look for new physics at low energies [37]. Loops are very sensitive to additional heavy particles, for example, charged Higgs, SUSY particles, or fourth generation particles. The inclusive $b \to s\gamma$ rate measured at CLEO has already placed constraints on charged Higgs models, and an anomalous $WW\gamma$ coupling, and other models (Sec. 4.2).

Non-standard models with four generations of quarks can, while respecting the experimental measurement of $b \to s\gamma$, significantly decrease the $b \to d\gamma$ electromagnetic penguin and $b \to d$ gluonic penguin rates while noticeably increasing the $b \to d$ electroweak and vertical penguin rates. Models with Z^0-mediated flavor-changing neutral currents can enhance $B^0 \to \ell^+\ell^-$ by two orders of magnitude over the Standard Model value and $B_s^0 \to \ell^+\ell^-$ by one order of magnitude. These models can also increase the electroweak penguin-dominated decays $B^+(B_s^0) \to \phi\pi^+(\phi\pi^0)$ by two (one) orders of magnitude above the SM prediction without violating the current limits on $b \to s\ell^+\ell^-$ or $B^0 \to K_S^0 K_S^0$. Multi-Higgs doublet models can also enhance the rates of di-lepton processes such as $B^0 \to \ell^+\ell^-$, and in particular, $b \to s\tau^+\tau^-$ can be enhanced without affecting $b \to s\mu^+\mu^-$ or $b \to se^+e^-$. In supersymmetric models, contributions from a charged Higgs in the penguin loop can be cancelled by contributions from charginos and gluinos in the loop, thus leaving $b \to s\gamma$ at the Standard Model value, while increasing the $b \to s\ell^+\ell^-$ rate. Similarly, if gluinos couple more readily to gluons than to photons, the $b \to sg^*$ rate can be strongly enhanced without affecting $b \to s\gamma$ [38]. In particularly favorable scenarios, SUSY "penguino" effects can dominate Standard Model penguin effects in decays such as $B^0 \to K^0\phi$ [39]. Even if new physics conspires to give the same rates as Standard Model predictions, there will likely be effects in CP violation. For instance London and Soni [36] point out that differences between the value of $\sin 2\beta$ measured from $B \to \psi K_S^0$ and the value measured from penguins such as $B^0 \to \eta' K_S^0$ might indicate the presence of non-SM processes. These are just a few of the many ways that new physics can be detected in B penguin decays.

Recently, there has been much discussion about new physics enhancing the $b \to sg^*$ rate [38, 40, 41, 42], thereby solving a couple of "mysteries" in B physics: the B semileptonic branching fraction is measured [43] to be smaller than theoretical predictions [44]; and the number of charm particles per B decay is smaller than predicted [45]. Both of these mysteries can be solved by increasing the non-leptonic, non-charm B width, e.g., $b \to sg^*$ which is so far not experimentally well-constrained. A rate of $\mathcal{O}(10\%)$ seems sufficient. However, limits on the $b \to sg^*$ rate are starting to rule out this explanation (Sec 5.4).

3 EXPERIMENTAL OVERVIEW

At present b quark decays are under investigation with high statistics data samples from three different colliders: the Cornell Electron-positron Storage Ring (CESR) producing $B\bar{B}$ pairs in decays of the $\Upsilon(4S)$ resonance just above the $e^+e^- \to B\bar{B}$ threshold; the Large Electron-Positron collider (LEP) at the European Laboratory for Particle Physics (CERN), which produced $b\bar{b}$ pairs in Z^0 decays; and the Tevatron at Fermi National Accelerator Laboratory (FNAL) producing $b\bar{b}$ pairs in $p\bar{p}$ collisions. Various production aspects of these machines are compared in Table 1.

Table 1: Various parameters characterizing experimental environments at three colliders used in analyses of b quark data. Explanation of the symbols: $\sigma-$cross section, $\mathcal{L}-$luminosity, $\beta-$velocity of b quarks, $\beta\gamma c\tau-$mean decay path, $f-$fractions of b hadron species produced.

Quantity	$\Upsilon(4S)$ (CESR)	Z^0 (LEP)	Tevatron
$\sigma(b\bar{b})$ (nb)	1.1	9.2	~ 30000 (~ 6000)†
$\sigma(b\bar{b})/\sigma(q\bar{q})$	~ 0.3	~ 0.2	~ 0.001
$\mathcal{L}^{peak}$ (10^{31} cm^{-2} s^{-1})	48.0	1.1	2.5
$\int \mathcal{L}dt$ (pb^{-1}) analyzed	3100	~ 120	~ 110
in pipeline	3600		
$b\bar{b}$ pairs analyzed (10^6)	3.3	0.9	~ 3300 (~ 660)†
β	~ 0.07	~ 1	~ 1
$\beta\gamma c\tau$ (μm)	30	2600	500
fragmentation background	no	some	large
B energy	$E_{\rm beam}$	$\sim 0.7\, E_{\rm beam}$	
spatial separation of b and $\bar{b}$	no	yes	yes
$f_{B^+} \approx f_{B^0}$	~ 0.5	~ 0.4	~ 0.4
$f_{B_s^0}$	–	~ 0.1	~ 0.1
f_{Λ_b}	–	~ 0.1	~ 0.1
main advantage	simple production, statistics	vertexing, one b at a time	cross-section, vertexing

$\dagger$ These numbers correspond to the central region, $|y| < 1$, with high transverse momentum of the b quark, $p_t > 6$ GeV (the number in parentheses).

CESR provides the highest luminosity and a simple production mechanism. Since no fragmentation particles are produced, the energy of reconstructed B's can be constrained to the beam energy which provides for a powerful reconstruction technique. Also, decay products from the two B's in the event populate the entire solid angle, allowing background discrimination based on event shape. However, since the two B mesons are produced almost at rest, detection of a detached secondary B decay vertex is not possible on an event-by-event basis.

At LEP, since the momentum of the b hadrons is appreciable, their decay

products are easily separated into back-to-back hemispheres. A large decay length gives rise to many important analysis techniques. Even though the $b\bar{b}$ cross section is much larger than at the $\Upsilon(4S)$ resonance, the high energy of the beam limits achievable luminosity. The small sample size is the limiting factor for the LEP experiments.

The main asset of the Tevatron experiments is their huge production cross-section. A large background cross-section is the main obstacle to overcome in these experiments. Specialized triggering is needed to limit data acquisition to manageable rates. So far, the results from the Tevatron have been mostly limited to channels containing high p_t muons. Again, vertexing is an important selection tool.

CESR houses only one experimental apparatus (CLEO II). There are four experiments at LEP (ALEPH, DELPHI, OPAL, and L3), and two at the Tevatron (CDF and D0). All these collider detectors have a similar "onion" structure. The beam collision point is surrounded by a thin vacuum pipe, followed by subsequent layers of nearly cylindrical detectors. Most of the experiments also have end-caps to maximize solid angle coverage. The innermost layer is created by a silicon strip vertex detector used to pinpoint production points of charged particles. The vertex detector is followed by a larger gaseous charged-particle tracker. Together they are used to determine particle momenta from curvature in a solenoidal magnetic field (except for D0 which has no magnetic field). In addition, most experiments measure specific ionization (dE/dx) in the tracking devices to obtain partial charged hadron identification. To aid particle identification and triggering, many detectors also have Time-of-Flight (ToF) scintillation counters surrounding the tracking system. The DELPHI experiment has a Ring Imaging Čerenkov instead, providing superior charged hadron identification. In the next layer, an electromagnetic calorimeter measures electron and photon energies by integrating over electromagnetic showers developing in a dense medium. Especially noteworthy are the CLEO II and L3 scintillating-crystal calorimeters, which have superb energy resolution. The final layer comprises a hadronic calorimeter which measures energies of charged and neutral hadrons. The calorimeters also identify muons which penetrate to the outermost layers. CLEO II has no hadron calorimeter; instead a thick layer of iron is used to identify muons.

In our article, we also refer to the previous generation of experiments at $\Upsilon(4S)$, CLEO I at CESR and ARGUS at DORIS (a CESR-like e^+e^- storage ring which operated at DESY in Hamburg), and in $p\bar{p}$ collisions, UA1 at Super Proton-antiproton Synchrotron (S$p\bar{p}$S) at CERN. The amount of data collected by these older experiments was about two orders of magnitude smaller than in the contemporary experiments.

Future B experiments are discussed in section 6.

4 ELECTROMAGNETIC PENGUINS

4.1 $B \to X\gamma$ Exclusive decay modes

After a b quark decays to $s\gamma$ via the penguin diagram (Fig. 2) the produced s quark and the spectator $\bar{q}$ ($\bar{q} = \bar{u}$ for B^-, and $\bar{d}$ for B^0) turn into hadrons. The final state usually contains one kaon and at least one pion ($B \to K\gamma$ is forbidden by angular momentum conservation). Hadronization may proceed via creation of an intermediate strange resonance: $K^*(892)$, $K_1(1270)$, $K_1(1400)$,

etc. The existence of penguin decays was first confirmed experimentally by the CLEO observation [46] of the exclusive decay $B \to K^*(892)\gamma$, with $K^* \to K\pi$. The initial observation was based on 1.5 million $e^+e^- \to \Upsilon(4S) \to B\bar{B}$ events. Reconstruction of exclusive final states from B mesons produced at the $\Upsilon(4S)$ benefits from the beam energy constraint: $E_B = E_{beam}$. Thus, energies of the B decay products must add up to the beam energy: $\Delta E = (E_{K^*} + E_\gamma) - E_{beam} \approx 0$. Also the B meson mass resolution is improved by an order of magnitude with the use of the beam constraint: $M_B = \sqrt{{E_{beam}}^2 - (\vec{p}_{K^*} + \vec{p}_\gamma)^2}$. These tight kinematic constraints are crucial in background suppression and signal extraction. Eleven signal events were observed over a background of two events, estimated from the ΔE and M_B sidebands.

Since the first observation, CLEO has presented an updated analysis based on larger statistics (2.6 million $B\bar{B}$ events in 2.4 fb^{-1} of integrated luminosity) and improved analysis techniques [47]. Instead of cutting on various variables to define the signal region, and then using sidebands to estimate the background, the improved analysis used a maximum likelihood fit to determine signal and background yields. In addition to M_B and ΔE, event shape variables and M_{K^*} also were used in the fit. The event shape information was optimized to distinguish between the signal and the dominant background due to continuum production of lighter quarks ($e^+e^- \to q\bar{q}$, $q = d, u, s, c$). This method improved the signal efficiency by a factor of two. Even though the background also increased, the signal sensitivity increased by about 30% beyond the gain from the increased integrated luminosity. Averaging over various charge modes ($K^+\pi^-$, $K^0_S\pi^0$, $K^0_S\pi^-$, $K^-\pi^0$) CLEO obtained: $\mathcal{B}(B \to K^*\gamma) = (4.2 \pm 0.8 \pm 0.6) \times 10^{-5}$. Projections of the maximum likelihood fit onto M_B, ΔE, and M_{K^*} are shown in Fig. 9 for the $K^+\pi^-$ channel which has the largest statistics.

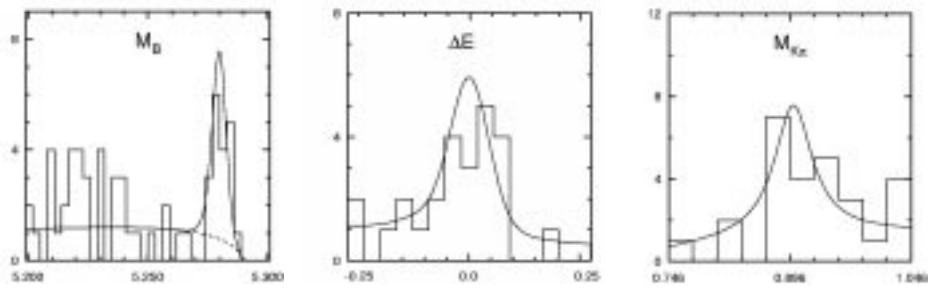

Figure 9: Projections of the maximum likelihood fit (solid lines) onto M_B, ΔE, and M_{K^*} for the $B^0 \to (K^+\pi^-)\gamma$ data (histograms). The horizontal scales are in GeV. The vertical scale gives number of events per bin.

The measured branching fraction is in the range predicted by the Standard Model, $(1 - 15) \times 10^{-5}$ [16]. It is also an order of magnitude larger than would be expected if the penguin diagram were not present [48].

LEP experiments looked for these decays in $e^+e^- \to Z^0 \to b\bar{b}$ data but were not able to observe the signal due to an insufficient number of $b\bar{b}$ pairs. They also looked for $B_s \to \phi\gamma$ decays. ALEPH set a 90% C.L. upper limit of 29×10^{-5} on the branching fraction for these decays [49].

4.2 Inclusive measurements of $b \to s\gamma$ rate

4.2.1 Experimental results

The measured rate for the exclusive mode $B \to K^*\gamma$ is in the ball-park of Standard Model predictions. Quantitative tests of the Standard Model with rates measured for exclusive channels are severely handicapped by our inability to calculate hadronization probabilities from the first principles of the theory. Predictions of phenomenological models for the K^* fraction in $b \to s\gamma$ decays, $R_{K^*} \equiv \mathcal{B}(B \to K^*\gamma)/\mathcal{B}(b \to s\gamma)$, vary from 1–40% [16]. One should notice improvement in recent lattice-QCD calculations in this area [19].

Fortunately, when summed over all possible final states, hadronization probabilities aren't relevant and the inclusively measured rate should reflect the short distance interactions which can be accurately predicted using the effective Hamiltonian of the Standard Model. Since the first non-perturbative correction is expected to be of second order in the Λ_{QCD}/m_b expansion, it should be small, thanks to the heavy b quark mass. Next-to-leading order perturbative calculations have been recently completed for $b \to s\gamma$. Assuming unitarity of the CKM matrix to constrain $|V_{ts}|$ the Standard Model predicts [12]: $\mathcal{B}(b \to s\gamma) = (3.5 \pm 0.3) \times 10^{-4}$.

When reconstructing simple exclusive final states such as $B \to K^*\gamma$, $K^* \to K\pi$, backgrounds are usually low due to tight kinematic constraints, in this case constraints to the B and K^* masses and the beam energy. Inclusive measurements are more challenging and they are often background limited.

The main background for CLEO is again from $e^+e^- \to q\bar{q}$ events. This background can be subtracted reliably with data taken below the $e^+e^- \to B\bar{B}$ threshold. However, statistical fluctuations in the background level can easily swamp the signal unless the background is efficiently suppressed. Backgrounds from B decays are less serious since $b \to s\gamma$ decays are quasi-two-body and produce higher energy photons ($E_\gamma \sim m_b/2$) than photons from typical B decay modes.

CLEO used two complementary approaches to suppress the continuum background [50]. In one approach only the photon among $b \to s\gamma$ decay products was explicitly reconstructed. Shape differences between $B\bar{B}$ events and $q\bar{q}$ background were used for background suppression. $B\bar{B}$ events are nearly spherical since the B mesons are nearly at rest at the $\Upsilon(4S)$, while $q\bar{q}$ events have a distinct two-jet appearance. For the best sensitivity all shape variables were combined withe the use of a neural-net technique. The signal amplitude was extracted from a one-parameter fit to the neural net output variable, with the signal shape and the $B\bar{B}$ backgrounds taken from Monte Carlo simulation, and the continuum background subtracted using the below-threshold data. In the second approach, all products of the $b \to s\gamma$ decay were reconstructed as in exclusive reconstruction. Thus, the constraints to the B mass and beam energy could be used. The final state recoiling against the photon, denoted X_s, was required to contain a kaon candidate (a charged track consistent with $K^\pm$ by dE/dx and ToF, or a $K^0_s \to \pi^+\pi^-$ candidate) and 1–4 pions (including at most one π^0). In Fig. 10, we show the photon energy spectra measured by CLEO with these two methods in a sample of 2.2×10^6 $B\bar{B}$ events. The first method has rather large continuum background but also high signal efficiency (32%). The second method is very good in suppressing continuum background, but the signal efficiency is much smaller (9%). The sensitivity of these two approaches is nearly equal, and the

measurements of signal amplitudes are only slightly correlated. After combining these two methods, CLEO measured $\mathcal{B}(b \to s\,\gamma) = (2.32 \pm 0.57 \pm 0.35) \times 10^{-4}$, in agreement with the Standard Model calculations.

The X_s mass distribution from the CLEO inclusive B-reconstruction analysis is shown in Fig. 12. A clear $K^*(892)$ peak is observed followed by a dip which is expected since the next excited kaon resonance is $K_1(1270)$. A broad enhancement at and above the $K_1(1270)$ is observed; this is also expected since many resonant states exist in this region. The present experimental statistics are insufficient to establish a positive signal for any of the resonances beyond $K^*(892)$ taken separately.

Combining the inclusive and the exclusive measurements, CLEO determines $R_{K^*} = (18.1 \pm 6.8)\%$ in agreement with some phenomenological estimates [16]. In particular the calculations which take the most from QCD, QCD sum rules [18] and recent lattice-QCD calculations [19], are in good agreement with the data.

Inclusive $b \to s\gamma$ decays also have been observed recently in $Z^0 \to b\bar{b}$ data by ALEPH [52]. The ALEPH analysis, based on 0.8 million $b\bar{b}$ pairs, searches for these decays by selecting events with a single high energy photon and a jet in the opposite hemisphere which is $b-$like from its observed detached vertex. The B hadron candidate in the photon hemisphere was reconstructed by combining the photon with other particles in the same hemisphere until the ensemble matches the B meson mass within the experimental resolution. The particles were selected by their probability of belonging to a B meson which was assigned according to their momenta and impact parameters at the interaction point. Up to eight particles were allowed in addition to the photon, including charged tracks, π^0 mesons, and K_L^0 mesons detected in the hadron calorimeter. Once the B candidate was reconstructed, the photon was boosted to its rest frame where the energy E_γ^* is nearly monochromatic for signal photons ($E_\gamma^* \sim m_b/2$). Further background suppression was achieved by imposing requirements on the boosted sphericity and photon angle in the rest frame of the B meson candidate.

To measure the background the sample was divided into eight subsamples, seven of which contained little $b \to s\gamma$ signal. The variables used for this division were: lateral shower size in the electromagnetic calorimeter to distinguish prompt photons from merged π^0 mesons; vertex detachment in the opposite hemisphere to distinguish $b\bar{b}$ events from $q\bar{q}$ backgrounds; and energy of the B candidate to discriminate against final state radiation background. The shapes of the contributing backgrounds (split into four major components) and of the $b \to s\gamma$ signal are computed from Monte Carlo while their normalizations are fixed by a fit to the E_γ^* distributions in the eight subsamples. Fig. 11a shows the E_γ^* distribution in the signal sensitive subsample for both the data and the background and Fig. 11b shows the data after background subtraction. The total reconstruction efficiency ($\sim 13\%$) is similar to the efficiency obtained in the CLEO inclusive B reconstruction analysis. In spite of 2.75 times fewer $b\bar{b}$ events, ALEPH is able to observe a significant inclusive signal. This should be attributed to a better suppression of the light quark backgrounds (the dominant background at the $\Upsilon(4S)$) by the detached vertex cuts. The background composition is illustrated in Fig. 11a. The branching fraction measured by ALEPH, $\mathcal{B}(b \to s\,\gamma) = (3.11 \pm 0.80 \pm 0.72) \times 10^{-4}$, is consistent with the CLEO measurement and the Standard Model predictions.

The other LEP experiments were not able to detect a $b \to s\,\gamma$ signal and set upper limits consistent with the CLEO and ALEPH measurements:

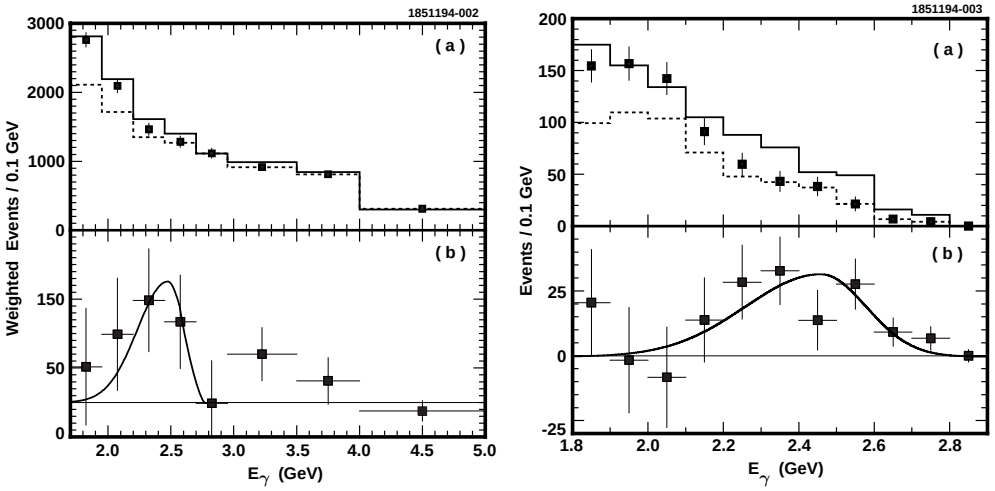

Figure 10: Inclusive E_γ spectra in the CLEO $b \to s\gamma$ measurement obtained with the event-shape analysis (left) and with inclusive B reconstruction (right). (a) $\Upsilon(4S)$ data (solid histogram), scaled below-threshold data (dashed histogram) plus estimated $\Upsilon(4S)$ backgrounds (points with error bars). (b) Background-subtracted data (points) and Monte Carlo prediction based on Ref. [51] for the shape of the $b \to s\,\gamma$ signal (solid curve). Note that the range of E_γ is very different for the left and right plots.

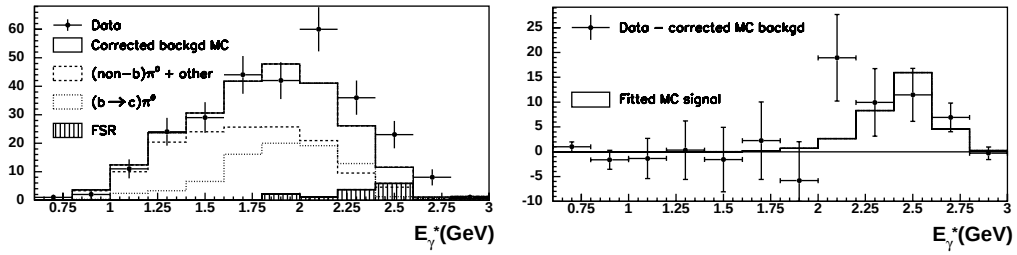

Figure 11: Inclusive E_γ^* spectrum in the ALEPH $b \to s\gamma$ measurement. On the left: data (points), total estimated background (solid histogram), π^0 background from $b \to c$ decays (dotted histogram), final state radiation background (shaded histogram), and all other backgrounds (dashed histogram). The latter comes mainly from π^0 decays from non-b sources and from η decays. On the right: background-subtracted data (points) and Monte Carlo prediction [51] for the shape of the $b \to s\,\gamma$ signal (solid histogram).

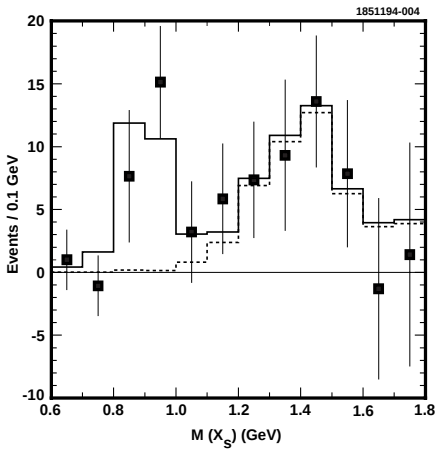

Figure 12: The X_s mass distribution in $B \to X_s\gamma$ decays from the CLEO inclusive B reconstruction analysis. The solid curve is a fit to the expected distribution from a spectator model. The dashed curve shows the non-$K^*(892)$ component of the fit.

DELPHI [53] $< 5.4 \times 10^{-4}$, L3 [54] $< 12 \times 10^{-4}$ (90% C.L.)

Combining the CLEO and the ALEPH results, we obtain:

$$\mathcal{B}(b \to s\,\gamma) = (2.54 \pm 0.57) \times 10^{-4}$$

4.2.2 Theoretical implications

Dividing the measured value of $\mathcal{B}(b \to s\,\gamma)$ by the Standard Model predictions, we obtain:

$$\left|\frac{V_{ts}^*}{V_{cb}} V_{tb}\right| = 0.85 \pm 0.10(\text{experiment}) \pm 0.04(\text{theory}) \ ,$$

consistent with the unitarity constraint [13]:

$$\left|\frac{V_{ts}^*}{V_{cb}} V_{tb}\right| \approx |V_{cs}| = 1.01 \pm 0.18$$

Using the measured values to eliminate $V_{tb} = 0.99 \pm 0.15$ [55] and $V_{cb} = 0.040 \pm 0.002$ [56], we obtain:

$$|V_{ts}| = 0.034 \pm 0.007$$

The agreement between the measured and the Standard Model rates (including the CKM matrix unitarity) leaves little room for non-standard contributions. For example, limits on anomalous $WW\gamma$ couplings can be obtained [57]. Such anomalous couplings can arise from internal structure of the gauge bosons or loop corrections involving new particles. They are parameterized by $\Delta\kappa$ and λ, which are both zero in the Standard Model. Non-zero values of these parameters would generate anomalous magnetic dipole and electric quadrupole moments of the W: $\mu_W = \frac{e}{2\,M_W}(2 + \Delta\kappa + \lambda)$, $Q_W^e = -\frac{e}{2\,M_W^2}(1 + \Delta\kappa - \lambda)$. They would either increase or decrease the $b \to s\,\gamma$ rate. The region of the $\Delta\kappa - \lambda$ space consistent with the CLEO measurement is shown in Fig. 13. The region allowed by a $p\bar{p} \to W\gamma\,X$ measurement by the D0 experiment [58] is also shown. The

two types of measurements are complementary. The $b \to s\,\gamma$ measurement alone excludes the $U(1)$ theory in which neutral bosons of electromagnetic and weak interactions do not mix.

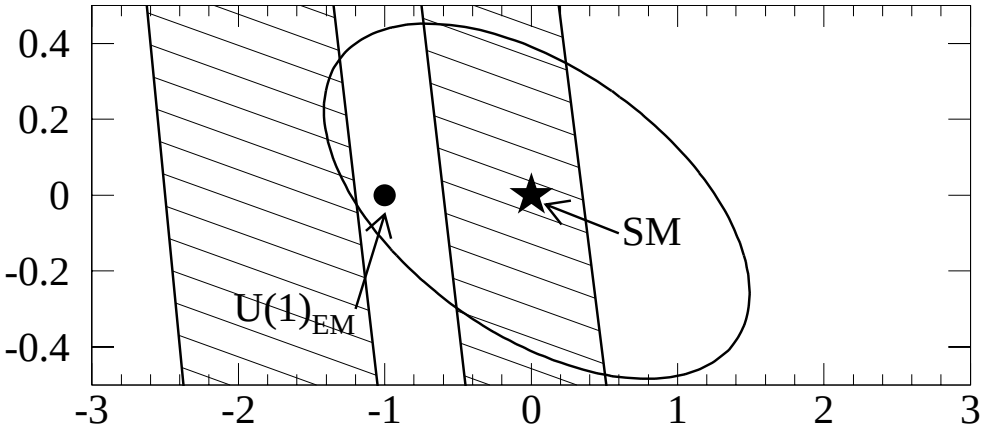

Figure 13: Limits on the anomalous $WW\gamma$ coupling parameters λ and $\Delta\kappa$. The hatched regions are consistent at 95% confidence level with the $b \to s\,\gamma$ rate measured by CLEO. The leading-log calculations, together with their uncertainties were used to obtain these bands [50]. The yield of $p\bar{p} \to W\gamma\,X$ measured by D0 limits the parameters to the interior of the ellipse (95% C.L.) [58]. The Standard Model (broken U(1)×SU(2)) and pure U(1) theory are displayed.

A charged Higgs boson can be exchanged instead of the charged W in the penguin loop. Models with two Higgs doublets are divided into two categories: Model I - both up-type and down-type quarks get their masses from the same Higgs doublet; Model II - up-type quarks get masses from one Higgs doublet, whereas down-type quarks get masses from the other Higgs doublet. The free parameters of these models are the mass of the exchanged Higgs and $\tan\beta$, which is the ratio of vacuum expectation values for the two Higgs doublets. In Model I the $b \to s\,\gamma$ rate is decreased relative to the Standard Model prediction. Since the CLEO measurement is somewhat below the Standard Model expectation, the data are consistent with Model I and a small Higgs mass. In Model II, the Higgs contribution always adds constructively to the Standard Model rate. Recently, next-to-leading order QCD corrections have been calculated for this model [14]. Using both the CLEO and ALEPH measurements, we obtain $\mathcal{B}(b \to s\,\gamma)/\mathcal{B}(b \to c l\nu) < 3.4 \times 10^{-3}$ (95% C.L.) which translates to a lower limit on the charged Higgs mass with slight $\tan\beta$ dependence: $M_H > 490$ GeV for $\tan\beta = 2$, as illustrated in Fig. 14. The limit is almost $\tan\beta$ independent for $\tan\beta \geq 2$.

Minimal supersymmetric extensions of the Standard Model (MSSM) include Model II charged Higgs doublets. However, the above lower limit on M_H does not directly apply to the supersymmetric model since a chargino-stop loop may destructively interfere with the charged Higgs and W-top contributions [59]. Nevertheless, the data impose interesting constraints on the minimal supersymmetry. Naively speaking, either charged Higgs, chargino and stop are all heavy or all light.

The limits on new physics imposed by the measurements can be expressed in a model independent way by bounds imposed on Wilson coefficients. The $b \to s\,\gamma$

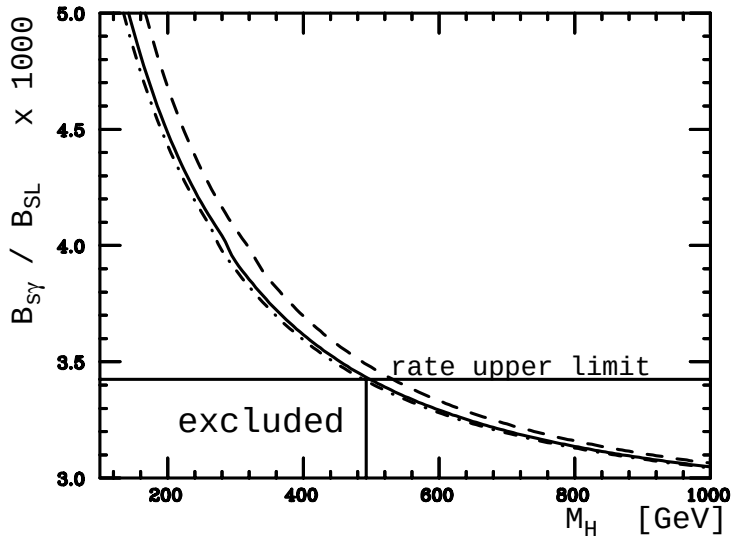

Figure 14: Exclusion region in the plane $\mathcal{B}(b \to s\gamma)/\mathcal{B}(b \to cl\nu)$ versus M_H for $\tan\beta = 1$ (dashed line), $\tan\beta = 2$ (solid line), and $\tan\beta = 5$ (dot-dashed line) as calculated by M. Ciuchini et al. [14] including next-to-leading QCD corrections and combining theoretical uncertainties linearly. The upper limit on $\mathcal{B}(b \to s\gamma)/\mathcal{B}(b \to cl\nu)$ is indicated (horizontal line), together with a corresponding lower limit on M_H for $\tan\beta = 2$ (vertical line).

decay rate is sensitive mostly to the value of the C_7 coefficient, with slight C_8 dependence as illustrated in Fig. 15 [60]. This figure also illustrates possible MSSM models, with additional theoretical symmetries motivated by supergravity. All of these models are made consistent with all direct searches for supersymmetric particles at LEP and the Tevatron. They are also out of reach of LEP-II. We see that the $b \to s\gamma$ results severely constrain the minimal supergravity models.

For constraints on other extensions of the Standard Model imposed by the measured $b \to s\,\gamma$ rate see e.g. Ref.[61].

4.3 $b \to d\gamma$ and V_{td}

Detection of $b \to d\,\gamma$ is difficult because the rates are suppressed by $|V_{td}|^2/|V_{ts}|^2$: $\mathcal{B}(B \to d\,\gamma) = (0.017 - 0.074) \times \mathcal{B}(B \to s\,\gamma)$ [62]. Rejection of the dominant background from $b \to s\,\gamma$ decays requires good particle identification, except for the simplest exclusive final states in which kinematic cuts alone are very effective. CLEO searched for $B \to (\rho,\omega)\,\gamma$ decays [47]. No evidence for the signal was found due to lack of sufficient experimental statistics (2.6×10^6 $B\bar{B}$ pairs). The following upper limits were set (90% C.L.): $\mathcal{B}(B^0 \to \rho^0\,\gamma) < 3.9 \times 10^{-5}$, $\mathcal{B}(B^0 \to \omega\,\gamma) < 1.3 \times 10^{-5}$, and $\mathcal{B}(B^- \to \rho^-\,\gamma) < 1.1 \times 10^{-5}$. The ratio $\mathcal{B}(B \to (\rho,\omega)\,\gamma)/\mathcal{B}(B \to K^*\gamma)$ can be used to determine $|V_{td}|^2/|V_{ts}|^2$ after corrections for phase space and $SU(3)-$flavor symmetry-breaking effects. Unfortunately the latter are somewhat model dependent. Long distance interactions may further complicate the analysis [63, 13]. From the present experimental limits CLEO obtains: $|V_{td}|^2/|V_{ts}|^2 < 0.45$–$0.56$, where the range indicates the uncertainty in the theoretical factors.

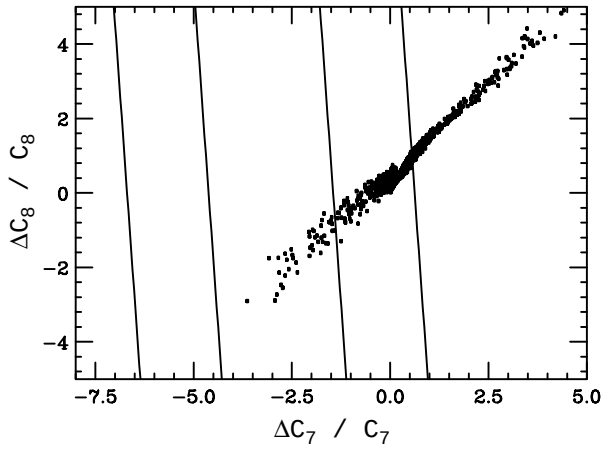

Figure 15: Bounds on the contributions from new physics to C_7 and C_8. The region allowed by the CLEO data corresponds to the area inside the two bands. Various minimal supergravity models consistent with the direct searches for supersymmetric particles at LEP and the Tevatron are represented by points [60].

4.4 $b \to s l^+ l^-$

In the Standard Model, the $b \to s l^+ l^-$ decay rate is expected to be nearly two orders of magnitude lower than the rate for $b \to s\,\gamma$ decays [13, 20]. Nevertheless, the $b \to s l^+ l^-$ process has received considerable attention since it offers a deeper insight into the effective Hamiltonian describing FCNC processes in B decays [13]. While $b \to s\,\gamma$ is only sensitive to the absolute value of the C_7 Wilson coefficient in the effective Hamiltonian, $b \to s l^+ l^-$ is also sensitive to the sign of C_7 and to the C_9 and C_{10} coefficients, where the relative contributions vary with $l^+ l^-$ mass. These three coefficients are related to the three different processes contributing to $b \to s\,l^+ l^-$: $b \to s\gamma^* \to s l^+ l^-$, $b \to s Z^* \to s l^+ l^-$, and the box diagram (see Fig. 3). Processes beyond the Standard Model can alter both the magnitude and the sign of the Wilson coefficients.

4.4.1 Searches in exclusive modes

The simplest allowed final states are $B \to K\, l^+ l^-$, and $B \to K^*\, l^+ l^-$. Each of them is expected to constitute $\sim$ 10% of the total $b \to s\, l^+ l^-$ rate. The most sensitive searches for these decays were performed by the CDF and CLEO experiments.

The CDF search [64] is based on 17.8 pb^{-1} of data ($\sim 5 \times 10^8\ b\bar{b}$ pairs for $|\eta| < 1$) and a di-muon trigger. The backgrounds are suppressed by transverse momentum cuts ($P_t(\mu_1) > 2$, $P_t(\mu_2) > 2.5$ GeV, $P_t(K^{(*)}) > 2$ GeV, $P_t(B) > 6$ GeV), a detached vertex cut ($c\tau(B) > 100\mu m$), an isolation requirement and a B mass cut. The resulting di-muon mass distributions are shown in Fig. 16. Signals from the decays $B \to K^{(*)}\psi^{(\prime)}$ can be seen. Since the branching fractions for these decays had been measured previously by other experiments, CDF used these signals for normalization. Reconstruction efficiencies are roughly 0.13% for the K, and 0.07% for the K^* modes. A few events observed outside the ψ (hatched) and ψ' (cross-hatched) bands are consistent with the background

estimates. They find the 90% C.L. upper limits $\mathcal{B}(B^- \to K^- \mu^+\mu^-) < 1.0 \times 10^{-5}$ and $\mathcal{B}(B^0 \to K^{*0} \mu^+\mu^-) < 2.5 \times 10^{-5}$.

The CLEO II experiment searched for these decays in a sample of $b\bar{b}$ pairs two orders of magnitude smaller ($\sim 2.2 \times 10^6$ $B\bar{B}$) than in the CDF analysis, though with efficiencies larger also by two orders of magnitude ($\sim 15\%$ for K and $\sim 5\%$ for K^*) and suitably low backgrounds. Thus, by coincidence, the sensitivity of the CDF and CLEO II experiments were very similar. In addition to the limits in the di-muon mode, $\mathcal{B}(B^- \to K^- \mu^+\mu^-) < 0.9\times10^{-5}$ and $\mathcal{B}(B^0 \to K^{*0} \mu^+\mu^-) < 3.1\times 10^{-5}$, CLEO also set limits using di-electrons: $\mathcal{B}(B^- \to K^- e^+e^-) < 1.2 \times 10^{-5}$ and $\mathcal{B}(B^0 \to K^{*0} e^+e^-) < 1.6 \times 10^{-5}$,

The experimental limits are an order of magnitude away from the Standard Model predictions.

4.4.2 Inclusive searches

The new CLEO analysis [65] looks for inclusive $b \to s\, l^+l^-$ decays using the inclusive B reconstruction technique previously described for $b \to s\,\gamma$ decays. The obtained di-lepton mass spectra are shown in Fig. 17. Again clear signals for $B \to X_s\psi$ and $B \to X_s\psi'$ are observed. Events outside the ψ and ψ' bands are consistent with $B\bar{B}$ background estimates (the $q\bar{q}$ background is small). With a sample of 3.3×10^6 $B\bar{B}$ pairs and reconstruction efficiencies around 5%, CLEO sets 90% C.L. upper limits, $\mathcal{B}(b \to s\, e^+e^-) < 5.7 \times 10^{-5}$ and $\mathcal{B}(b \to s\,\mu^+\mu^-) < 5.8 \times 10^{-5}$ (combined: $\mathcal{B}(b \to s\, l^+l^-) < 4.2 \times 10^{-5}$), The SM predictions [20], $\mathcal{B}(b \to s\, e^+e^-) = (0.8 \pm 0.2) \times 10^{-5}$ and $\mathcal{B}(b \to s\,\mu^+\mu^-) = (0.6 \pm 0.1) \times 10^{-5}$, are again an order of magnitude below the experimental limits.

The upper limit on inclusive $b \to s\,\mu^+\mu^-$ previously presented by the UA1 experiment at $Sp\bar{p}S$ collider [66] has been shown recently to be based on over-estimated sensitivity [65, 67]. A similar analysis recently completed by the D0 experiment at the Tevatron resulted in a less stringent limit, $< 32 \times 10^{-5}$ [67], than achieved by CLEO.

4.5 $b \to s\nu\bar{\nu}$

The rate for $b \to s\nu\bar{\nu}$ is enhanced compared to the $b \to s\, l^+l^-$ decays primarily by summing over three neutrino flavors ($b \to s\tau^+\tau^-$ has a small expected rate and will be difficult to detect experimentally). The predicted rate is only a factor of ten lower than for $b \to s\,\gamma$ [21]: $(3.8 \pm 0.8) \times 10^{-5}$. In principle, these decays are the cleanest theoretically among all penguin decays. Therefore, a measurement of the inclusive rate for this process would be of considerable interest. Unfortunately, the neutrinos escape detection making it difficult for experimentalists to control the backgrounds. So far, only LEP experiments have been able to probe these decays by requiring very large missing energy in a hemisphere [68, 69]. Semileptonic backgrounds are reduced by eliminating events with an identified lepton in the signal hemisphere. A detached vertex in the opposite hemisphere suppresses non-$b\bar{b}$ backgrounds. The missing energy distribution in a $b-$hemisphere obtained by ALEPH [68] in a sample of $\sim 0.5 \times 10^6$ $b\bar{b}$ pairs is shown in Fig. 18. A signal would be seen as an excess of events at large missing energy. The lack of such an excess is used by ALEPH to obtain a 90% C.L. limit, $\mathcal{B}(b \to s\,\nu\bar{\nu}) < 7.7 \times 10^{-4}$.

The exclusive mode $B \to K^*\,\nu\bar{\nu}$ is expected to constitute about 30% of the

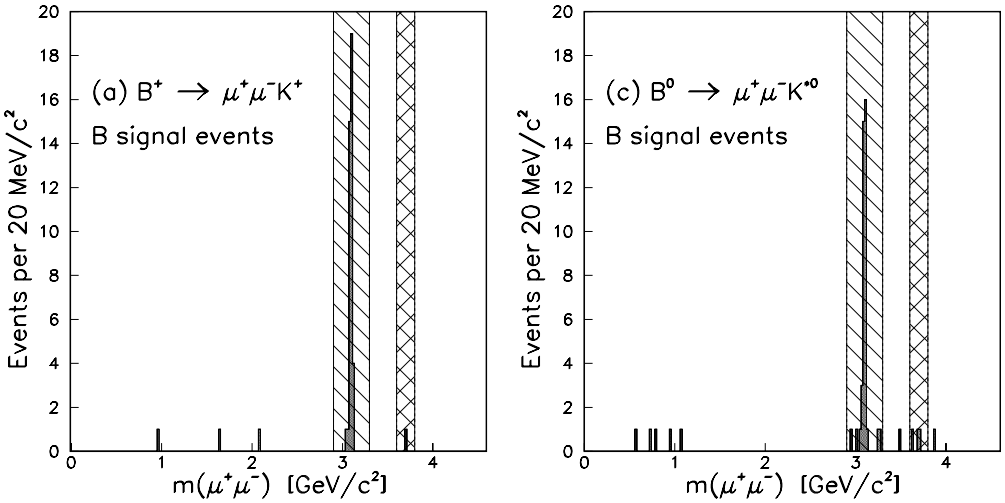

Figure 16: Di-muon mass distributions in the CDF search for $b \to s\,\mu^+\mu^-$ via **exclusive** final states $B^+ \to K^+\,\mu^+\mu^-$ (left) and $B^0 \to K^{*0}\,\mu^+\mu^-$ (right).

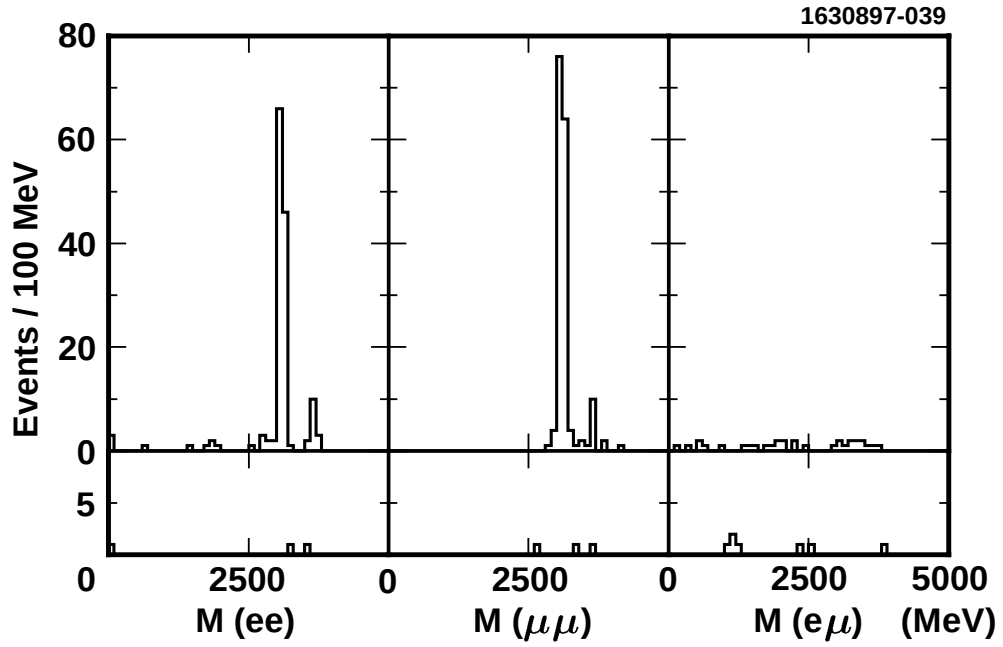

Figure 17: Di-lepton mass distribution in the CLEO **inclusive** search for $b \to s\,l^+l^-$. On-resonance (top) and below-threshold (bottom) data are shown.

total rate [17]. DELPHI obtains 90% C.L upper limits [53]: $\mathcal{B}(B^0 \to K^{*0}\nu\bar{\nu}) < 1.0 \times 10^{-3}$ and $\mathcal{B}(B_s \to \phi\,\nu\bar{\nu}) < 5.4 \times 10^{-3}$.

The inclusive limit set by ALEPH is an order of magnitude away from the expected rate. Unfortunately, no more data are expected at the Z^0 peak at LEP. Perhaps $\Upsilon(4S)$ experiments will be able to develop analysis techniques which can probe these decays with future high statistics data samples. It is hard to imagine that experiments at hadronic colliders will ever have any sensitivity to these decays.

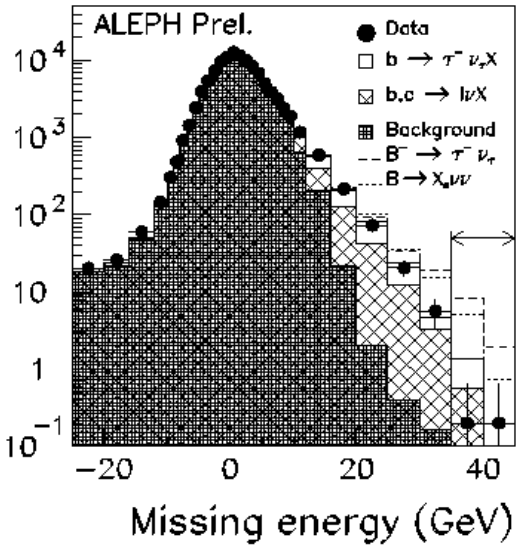

Figure 18: Missing energy in a hemisphere for the selected $b\bar{b}$ events by ALEPH (points). Shaded histograms show the estimated background distribution. The expected $b \to s\,\nu\bar{\nu}$ signal shape is indicated by a dotted line. The two highest bins are used to set the upper limit.

4.6 $B \to \gamma\gamma$

The vertical penguin $B^0(B_s^0) \to \gamma\gamma$ (Fig. 4a) decay rate is expected to be of order 10^{-8} (10^{-7}) [70, 71]. QCD corrections have been found to enhance the $B_s^0 \to \gamma\gamma$ rate by $\sim 50\%$ [71]. The L3 detector at LEP has a high resolution calorimeter, which is well suited to this analysis, with a photon resolution better than 2% for energies greater than 1 GeV [72]. Using their B-enriched data sample, L3 looks for pairs of high momentum photons with invariant mass near the B mass. The data are fit simultaneously for B^0 and B_s^0 signals with an exponential background. (No candidates are found in a $\pm 2\sigma$ mass window.) The L3 90% C.L. upper limits are given in Table 2. Unfortunately, these limits are several orders of magnitude away from constraining new physics.

Table 2: Results for vertical penguins. We give the 90% confidence level upper limit on the branching fractions (UL $\mathcal{B}$) and the theoretical predictions.

B^0 decay mode	Exp.	UL $\mathcal{B}$ (10^{-6})	Theory	B_s decay mode	Exp.	UL $\mathcal{B}$ (10^{-6})	Theory
$\gamma\gamma$	L3	38	10^{-8}	$\gamma\gamma$	L3	148	10^{-7}
e^+e^-	CLEOII	5.9	10^{-15}	e^+e^-	L3	54	10^{-14}
$\mu^+\mu^-$	CDF	0.68	10^{-10}	$\mu^+\mu^-$	CDF	2	10^{-9}
$\tau^+\tau^-$			10^{-8}	$\tau^+\tau^-$			10^{-7}

4.7 $B \to \ell^+\ell^-$

The Standard Model predictions [70] for $B \to \ell^+\ell^-$ are given in Table 2. The search for $B^0 \to e^+e^-$ and $B^0 \to \mu^+\mu^-$ at CLEO [73] is similar to their other rare B decay searches. The small background is suppressed using mild event shape requirements. No signal events are observed in either channel giving limits on each channel of 5.9×10^{-6}.

Since the CDF experiment has excellent muon identification and a muon trigger, $B \to \mu^+\mu^-$ decays could be recorded with good efficiency [74]. B_s^0 mesons are also produced at CDF. Background rejection is achieved using a detached vertex and an isolation requirement. In the CDF Run IA and IB data sample (≈ 100 pb^{-1}) they find one candidate which falls into both the B^0 and B_s^0 mass windows. This event is consistent with background, but is assumed to be signal for calculating upper limits. Results are included in Table 2.

Searches for $B \to \ell^+\ell^-$ have also been done by L3 [75]. The small background is suppressed by requiring large B energy. They observe no significant signals and fit the data simultaneously for B^0 and B_s^0 to extract upper limits on the branching fractions. The L3 limits for $B^0 \to e^+e^-$ ($\mu^+\mu^-$) are $1.4(1.0) \times 10^{-5}$, less stringent than the CLEO and CDF limits. The L3 limit for $B_s^0 \to e^+e^-$ is 5.4×10^{-5}, the only limit for this mode. Their limit for $B_s^0 \to \mu^+\mu^-$, 3.8×10^{-5}, is less restrictive than the CDF limit.

5 GLUONIC PENGUINS

Some representative Feynman diagrams relevant for charmless hadronic B decays are shown in Fig. 19. In addition to the penguin diagrams of primary interest in this review, we indicate examples of $b \to u$ tree diagrams in Fig. 19c, d, and g. Such diagrams are suppressed for decays with a strange particle in the final state but are dominant for many decays with no strange particle. Since penguins play a significant role in such decays without strange particles and the two processes can be difficult to separate experimentally, we will include results for both processes in our discussion. However we do not include results for decays involving the dominant $b \to c$ decay mechanism.

The first indication of signals in charmless hadronic B decays came in a 1993 CLEO publication [76] in which a quite significant signal was found for $B \to h^+h^-$, where h is either K or π. Statistics were not sufficient to obtain significant signals for $B^0 \to K^+\pi^-$ or $B^0 \to \pi^+\pi^-$ separately. Subsequently CLEO updated these results [77], still without an observation of either mode individually, and provided limits for many related modes.

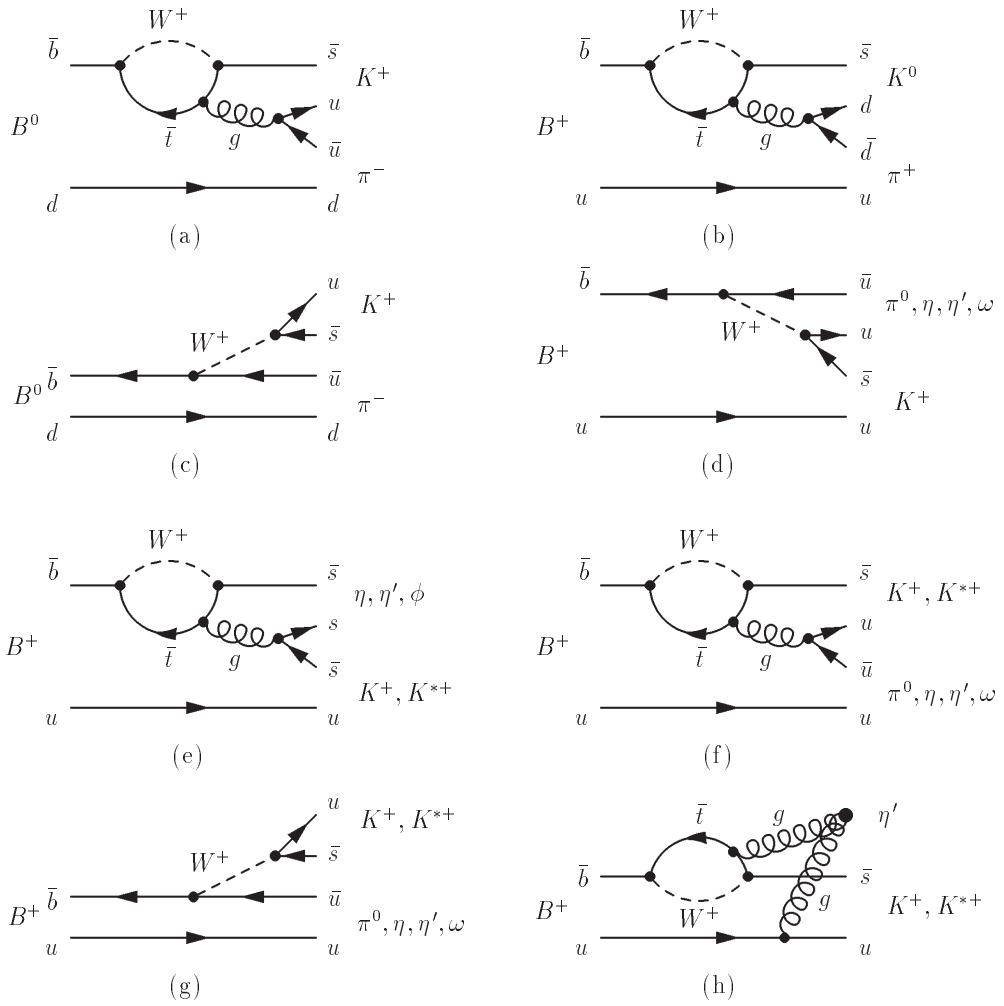

Figure 19: Feynman diagrams for some of the penguin and tree processes which are expected to be dominant for the modes described in this paper.

Several LEP experiments have used the excellent vertex resolution provided by their silicon vertex detectors to obtain virtually background-free evidence for charmless hadronic B decays. Examples of such events are shown in Fig. 5 for the ALEPH experiment [78]. The LEP experiments also have some ambiguity between the decays $B^0 \to K^+\pi^-$, $B^0 \to \pi^+\pi^-$, and $B_s^0 \to K^+K^-$. Fig. 21 shows the mass distribution for ten candidate charmless hadronic B decays from the DELPHI experiment [53]. The final states include $\pi^+\pi^-$, $K^+\pi^-$, K^+K^-, $\rho^0\pi^+$, $K^{*0}\pi^+$, $K^+\rho^0$, and $K^+a_1^-$.

5.1 Exclusive decays of B mesons

In this section we discuss the recent observation of several new decay modes by CLEO and many upper limits which are beginning to approach theoretical expectations.

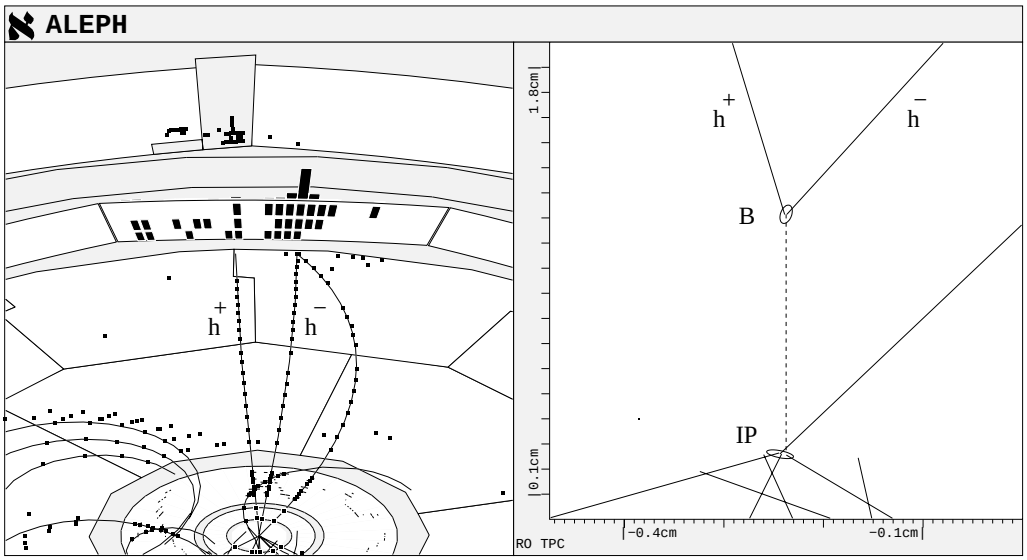

Figure 20: Event from the ALEPH experiment showing a $B^0 \to K^+\pi^-$ decay candidate as reconstructed with use of the ALEPH silicon vertex detector.

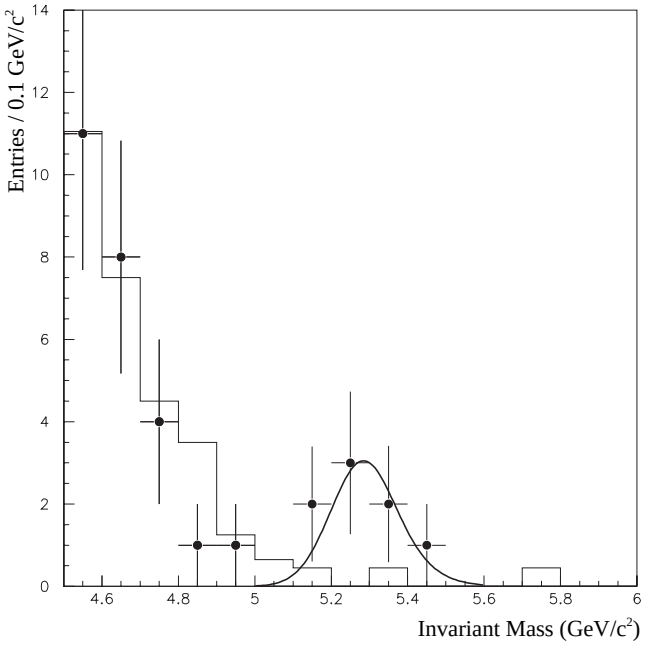

Figure 21: Invariant mass distribution obtained by DELPHI for ten charmless hadronic B decay candidates, background events at lower mass, and the Monte Carlo expectation for the background.

5.1.1 Experimental method

In addition to the 3.3 million $B\bar{B}$ pairs from $\Upsilon(4S)$ running (see Table 1), a sample of events obtained at a center-of-mass energy below $B\bar{B}$ threshold is used for studies of backgrounds from continuum $q\bar{q}$ production. Resonance states are reconstructed from charged tracks and photons with the decay channels: $\eta' \to \eta\pi^+\pi^-$, $\eta' \to \rho^0\gamma$, K^0 via $K_S \to \pi^+\pi^-$, $\rho^0 \to \pi^+\pi^-$, $\rho^+ \to \pi^+\pi^0$, $\pi^0 \to \gamma\gamma$, $\eta \to \gamma\gamma$, $\eta \to \pi^+\pi^-\pi^0$, $\omega \to \pi^+\pi^-\pi^0$, $\phi \to K^+K^-$, $K^{*0} \to K^+\pi^-$, $K^{*+} \to K^+\pi^0$, and $K^{*+} \to K^0\pi^+$.

The primary means of identification of B meson candidates is through their measured mass and energy. The dominant background process for all decays considered here is continuum $e^+e^- \to q\bar{q}$ production. Signal events have a total energy consistent with the beam energy (5290 MeV), while most background events have smaller energy. As discussed in Sec. 4.1, CLEO uses the variable $\Delta E = E_{\rm cand} - E_{\rm beam}$, which peaks at or near zero for signal events. Signal events also have mass M consistent with m_B (5280 MeV), only 10 MeV below the maximum value, while most background events have much smaller mass. For states decaying to the resonances mentioned above, the resonance mass is also important in discriminating against background processes. In the case of vector-pseudoscalar decays and the $\eta' \to \rho^0\gamma$ channel, the helicity angle distribution is also used. For modes with a high-momentum charged track or a charged track paired with a π^0, dE/dx information is also used to identify the charged track as a pion or kaon.

The large $q\bar{q}$ background can be reduced by about an order of magnitude with the use of event shape information. Since B mesons are produced nearly at rest, $B\bar{B}$ events tend to be spherical, whereas $q\bar{q}$ events tend to be quite collimated ("jetty").

In order to keep the efficiency high while still effectively rejecting $q\bar{q}$ background, a maximum likelihood (ML) fit has been performed for all of the recent CLEO analyses. The inputs to the fit are the quantities discussed in the previous two paragraphs, while the outputs are the number of signal and background events. This procedure provides an efficiency of 20-50% for most modes, at least a factor of two larger than previous CLEO and ARGUS analyses, with a comparable effective background.

5.1.2 $B \to K\pi$ and related decays

The simplest modes, both experimentally and theoretically are the decays to two-body final states without resonances. This includes $K\pi$ and $\pi\pi$ final states with both charged and neutral pions. The CLEO results [79] include observation of the decay $B^0 \to K^+\pi^-$, strong evidence for the decay $B^+ \to K^0\pi^+$, and limits for the other five final states. The signals are summarized in Table 3; the limits for the penguin modes are summarized in Table 4 while those for the modes dominated by $b \to u$ processes are included in Table 5.

Fig. 22 shows the likelihood contours for the three cases with significance greater than three standard deviations. While the significance for the $K^+\pi^0$ and $\pi^+\pi^0$ final states are both below 3σ, there is strong evidence for their sum ($h\pi^0$). This is similar to the case of the h^+h^- final state several years ago [76]. Fig. 23 shows projections of the fit onto the M and ΔE axes; for all projection plots, cuts have been made on other ML variables to better reflect the background

near the signal region.

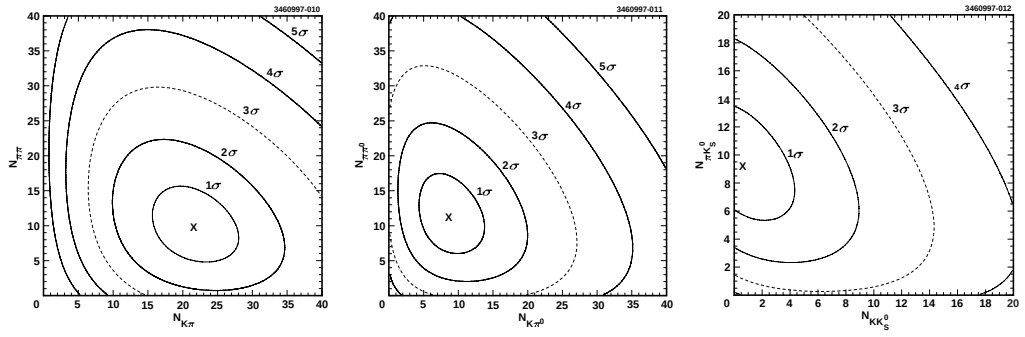

Figure 22: Likelihood contours for: (a) $B^0 \to K^+\pi^-$ and $B^0 \to \pi^+\pi^-$; (b) $B^+ \to K^+\pi^0$ and $B^+ \to \pi^+\pi^0$; (c) $B^+ \to \bar{K}^0 K^+$ and $B^+ \to K^0\pi^+$.

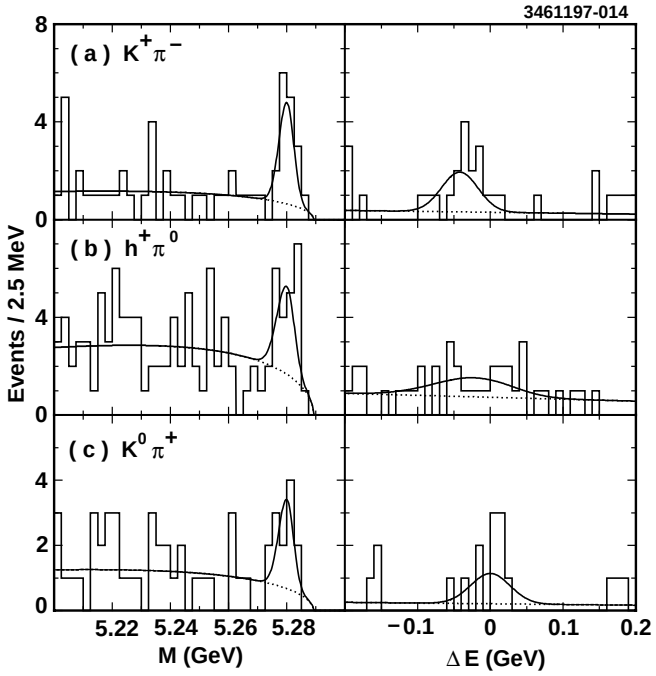

Figure 23: M and ΔE plots for (a) $B^0 \to K^+\pi^-$, (b) $B^+ \to h^+\pi^0$, and (c) $B^+ \to K^0\pi^+$. The scaled projection of the total likelihood fit (solid curve) and the continuum background component (dotted curve) are overlaid.

Note that all of the decay modes summarized in Table 3, some of which will be discussed in the next section, are decays which are expected to be dominated by penguins. There is still no direct evidence for the $b \to u$ tree modes, though signals with significance of more than two standard deviations in the $\pi^+\pi^-$ and $\pi^+\pi^0$ channels suggest that such decays may be observed soon. This dominance of penguins over $b \to u$ channels suggests that the problem of penguin pollution in CP violation measurements for modes such as $B^0 \to \pi^+\pi^-$ may be particularly severe.

While few conclusions can be reached with the present level of precision in the

Table 3: Results for the five decay modes which have signals with significance larger than 3σ. The second efficiency column includes B_r, the product branching fraction of resonance secondary decays.

Decay mode	Signal events	Signif.	$\epsilon(\%)$	$\epsilon\mathcal{B}_r(\%)$	$\mathcal{B}(10^{-5})$	Theory $\mathcal{B}(10^{-5})$
$B^0 \to K^+\pi^-$	$21.6^{+6.8}_{-6.0}$	$5.6\sigma^\dagger$	44	44	$1.5^{+0.5}_{-0.4} \pm 0.1$	0.1–2.4
$B^+ \to K^0\pi^+$	$9.2^{+4.3}_{-3.8}$	$3.2\sigma^\dagger$	35	12	$2.3^{+1.1}_{-1.0} \pm 0.4$	0.5–2.0
$B^+ \to \eta' K^+$	$33.1^{+8.1}_{-6.8}$	7.5σ	28	15	$6.5^{+1.5}_{-1.4} \pm 0.9$	0.7–4.1
$B^0 \to \eta' K^0$	$7.1^{+4.1}_{-3.0}$	3.8σ	25	4	$4.7^{+2.7}_{-2.0} \pm 0.9$	0.9–3.3
$B^+ \to \omega K^+$	$12.2^{+5.5}_{-4.5}$	3.9σ	28	25	$1.5^{+0.7}_{-0.6} \pm 0.2$	0.1–0.7

† The significance does not include systematic uncertainties.

$K\pi$ system, Fleischer and Dighe, Gronau and Rosner [33] have pointed out the promise of such decays for measurements of the weak phases α and γ. This is of great importance since these are the two phases that will be hardest to measure with time-dependent asymmetry techniques at BaBar and Belle. Subsequently Fleischer and Mannel [92] pointed out that if the ratio

$$R = \frac{\mathcal{B}(B^0 \to K^+\pi^-) + \mathcal{B}(\bar{B}^0 \to K^-\pi^+)}{\mathcal{B}(B^+ \to K^0\pi^+) + \mathcal{B}(B^- \to \bar{K}^0\pi^-)} \tag{4}$$

is significantly smaller than 1, useful bounds can be placed on the weak phase γ, namely $\sin^2\gamma < R$. From Table 3, we find $R = 0.65 \pm 0.38$, indeed less than 1 but certainly not significantly so. Improvements upon the original concept have recently been suggested [93, 94]. There are potential complications in this analysis due to SU(3) symmetry-breaking effects, electroweak penguins and especially final-state interactions as discussed recently by many authors [94, 95]. The situation is not yet resolved but it appears promising that future measurements of these decay rates, with samples 10-100 times larger than existing samples, may be able to constrain the CP phase γ.

There is considerable interest in the CP asymmetry for these and other decay modes. However, since the observed samples are so small, experimentalists cannot yet make meaningful measurements. The asymmetry, $A \equiv \frac{(N_+ - N_-)}{(N_+ + N_-)}$, where N_+ and N_- are the number of K^+ and K^- events respectively, is a measure of direct CP violation. For most modes, predictions are $A \sim 0.1$, while experimental errors are presently greater than 0.3.

5.1.3 $B \to \eta' K$, $B \to \omega K$ and related decays

Decays with resonances tend to be more difficult to observe because more particles are involved and the secondary branching fractions to observable final states are frequently below 50%. The observation of signals for $B \to \eta' K$ [88] and $B \to \omega K$ [89] was unexpected, since previous predictions were that the branching fractions would be smaller than that observed by at least a factor of two.

CLEO finds a strong signal for $B^+ \to \eta' K^+$ in both the $\eta' \to \eta\pi^+\pi^-$ (5.2σ) and $\eta' \to \rho^0\gamma$ (4.8σ) channels. Combining these with evidence from the chain

Table 4: Results from measurements of penguin-candidate B decay modes. We give the 90% confidence level upper limit on the branching fractions (UL $\mathcal{B}$), and the range of theoretical predictions [80, 81, 82]. K^*, K_1 and K_2^* are shorthand designations for $K^*(892)$, $K_1(1400)$ and $K_2^*(1430)$, respectively. Modes indicated by "**" have been observed (see Table 3). Limits below the upper end of the theoretical range are indicated in bold face. Experiment key: AR (ARGUS [86]), C1 (CLEO I [87]), C2 (CLEO II [77, 79, 88, 89]), D (DELPHI [53]).

B^0 final state	Expt.	UL $\mathcal{B}$ (10^{-6})	Theory (10^{-6})	B^+ final state	Expt.	UL $\mathcal{B}$ (10^{-6})	Theory (10^{-6})
$K^+\pi^-$	C2	**	1–26	$K^+\pi^0$	C2	16	3–15
$K^0\pi^0$	C2	41	2–10	$K^0\pi^+$	C2	**	5–36
K^+K^-	C2	4		K^+K^0	C2	21	0.6–3
K^0K^0	C2	17	0.6–1.4				
$K^{*+}\pi^-$	C2	72	1–19	$K^{*+}\pi^0$	C2	99	0.5–9
$K^{*0}\pi^0$	C2	28	1–5	$K^{*0}\pi^+$	C2	41	4–12
$K^{*0}K^0$			0.3–1	$K^{*+}K^0$			0.0005–0.04
$K^{*+}K^-$				$K^{*0}K^+$			0.3–1
$K^{*0}K^{*0}$			0.3–1	$K^{*+}K^{*0}$			0.3–1
$K^+\rho^-$	C2	35	0.2–2	$K^+\rho^0$	C2	19	0.1–2
$K^0\rho^0$	C2	39	0.04–0.8	$K^0\rho^+$	C2	48	0.01–0.4
$K^{*0}\rho^0$	AR	460	0.5–6	$K^{*+}\rho^0$	AR	900	0.06–8
$K^{*+}\rho^-$			0.3–18	$K^{*0}\rho^+$			5–13
$K^0\eta$	C2	33	0.07–3	$K^+\eta$	C2	14	0.2–5
$K^{*0}\eta$	C2	30	0.03–9	$K^{*+}\eta$	C2	30	0.2–6
$K^0\eta'$	C2	**	9–41	$K^+\eta'$	C2	**	7–65
$K^{*0}\eta'$	C2	39	0.05–8	$K^{*+}\eta'$	C2	130	0.03–1.5
$K^0\omega$	C2	57	0.02–10	$K^+\omega$	C2	**	0.2–13
$K^{*0}\omega$	C2	23	0.6–12	$K^{*+}\omega$	C2	87	0.4–15
K^0f_0	C1	360		K^+f_0	C1	80	
$K^{*0}f_0$	C1	170					
$K_1^+\pi^-$	AR	1100		$K_1^0\pi^+$	AR	2600	
$K_1^0\rho^0$	AR	3000		$K_1^+\rho^0$	AR	780	
$K_2^{*+}\pi^-$	AR	2600		$K_2^{*0}\pi^+$	AR	680	
$K_2^{*0}\rho^0$	AR	1100		$K_2^{*+}\rho^0$	AR	1500	
$K^+a_1^-$	D	230					
$K^0\phi$	C2	31	0.3–18	$K^+\phi$	C2	**5**	0.3–14
$K^{*0}\phi$	C2	**21**	0.2–31	$K^{*+}\phi$	C2	41	0.2–31
$K_1^0\phi$	AR	5000	21	$K_1^+\phi$	AR	1100	21
$K_2^{*0}\phi$	AR	1400	0.7	$K_2^{*+}\phi$	AR	3400	0.7
$\pi^0\phi$	C2	5	0.002–0.2	$\pi^+\phi$	C2	5	0.005–0.4
$\rho^0\phi$	C2	13	0.002–0.3	$\rho^+\phi$	C2	16	0.004–0.5
$\eta\phi$	C2	9	0.001–0.1				
$\eta'\phi$	C2	31	0.001–0.1				
$\omega\phi$	C2	21	0.002–0.3				
$\phi\phi$	C2	12					
				$\bar{\Lambda}p$	C1	60	

Table 5: Results from measurements of other charmless B decays. We give the 90% confidence level upper limit on the branching fractions (UL $\mathcal{B}$), and the range of theoretical predictions [80, 81, 82]. Limits below the upper end of the theoretical range are indicated in bold face. Experiment key: AL (ALEPH [78]), AR (ARGUS [90]), C1 (CLEO I [91]), C2 (CLEO II [77, 79, 88, 89]).

B^0 decay mode	Expt.	UL $\mathcal{B}$ (10^{-6})	Theory (10^{-6})	B^+ decay mode	Expt.	UL $\mathcal{B}$ (10^{-6})	Theory (10^{-6})
$\pi^+\pi^-$	C2	**15**	7–18	$\pi^+\pi^0$	C2	20	3–20
$\pi^0\pi^0$	C2	9	0.1–1.3				
$\rho^\pm\pi^\mp$	C2	88	26–52	$\rho^+\pi^0$	C2	77	11–27
$\rho^0\pi^0$	C2	24	0.9–2	$\rho^0\pi^+$	AL	32	0.4–8
$\rho^+\rho^-$	AR	2200	13–34	$\rho^+\rho^0$	AL	120	6–23
$\rho^0\rho^0$	AL	40	0.5–3				
$\eta\pi^0$	C2	8	0.2–4	$\eta\pi^+$	C2	15	1.9–8
$\eta\rho^0$	C2	13	0.02–7	$\eta\rho^+$	C2	32	4–17
$\eta'\pi^0$	C2	**11**	0.06–14	$\eta'\pi^+$	C2	31	1–23
$\eta'\rho^0$	C2	23	0.001–11	$\eta'\rho^+$	C2	47	3–24
$\eta\eta$	C2	18	0.06–2				
$\eta'\eta$	C2	27	0.08–10				
$\eta'\eta'$	C2	47	0.02–14				
$\omega\pi^0$	C2	14	0.01–12	$\omega\pi^+$	C2	23	0.6–8
$\omega\rho^0$	C2	11	0.005–0.4	$\omega\rho^+$	C2	61	7–26
$\omega\eta$	C2	12	0.05–7				
$\omega\eta'$	C2	60	0.02–19				
$\omega\omega$	C2	19	0.1–3				
$f_0\pi^0$				$f_0\pi^+$	C1	140	
$f_2\pi^0$				$f_2\pi^+$	C1	240	
$a_1^\pm\pi^\mp$	AL	240		$a_1^0\pi^+$	AR	900	
$a_1^0\pi^0$	AR	1100		$a_1^+\pi^0$	AR	1700	
$a_2^\pm\pi^\mp$	C1	300					
$a_1^0\rho^0$	AR	2400		$a_1^+\rho^0$	AL	130	
$a_1^\pm\rho^\mp$	AR	3400		$a_1^0\rho^+$			
$a_1^+a_1^-$	AL	570		$a_1^+a_1^0$	AR	13000	
$p\bar{p}$	AL	18	0.5–4				
$\Delta^0\bar{\Delta}^0$	AL	380		$\Delta^0\bar{p}$	AL	76	
$\Delta^{++}\bar{\Delta}^{--}$	AL	47		$\Delta^{++}\bar{p}$	AL	**26**	0.1–130

$\eta' \to \eta\pi^+\pi^-$, $\eta \to \pi^+\pi^-\pi^0$ yields a significance (including systematic errors in the yield) of 7.5σ as shown in Fig. 24a. The combined significance for the $B^0 \to \eta' K^0$ decay is 3.8σ as shown in Fig. 25a. Projections onto the B mass axis are also shown.

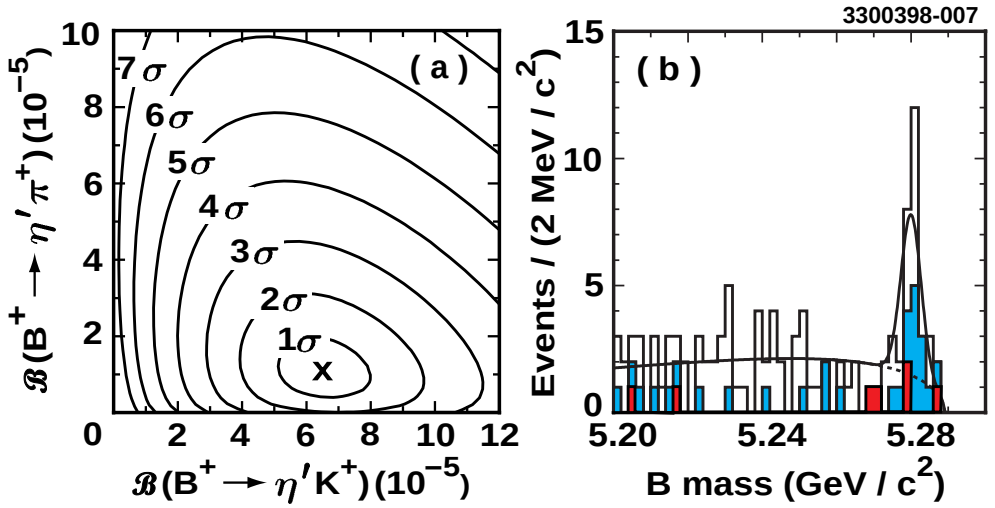

Figure 24: (a) Likelihood contours and (b) mass projection plot for $B^+ \to \eta' h^+$. For (b), the curves are an overlay of the best fit function (solid) and background component (dashed). The histograms show submodes: $\eta' \to \eta\pi\pi$ ($\eta \to \pi^+\pi^-\pi^0$, dark shaded), $\eta' \to \eta\pi\pi$ ($\eta \to \gamma\gamma$, light shaded), and $\eta' \to \rho\gamma$ (open).

Similarly, CLEO finds a signal with 3.9σ significance for $B^+ \to \omega K^+$ as shown in Fig. 26. The mass projection plot is also shown. The results for all three signals are summarized in Table 3. As in the previous section, there are hints of signals for the corresponding tree decay modes $B^+ \to \eta'\pi^+$ and $B^+ \to \omega\pi^+$, but the significance of each is only about 2σ.

The recent CLEO work includes limits on many other modes involving η, η', ω and ϕ mesons. Tables 4 and 5 summarize these and other results. The subset of these results from the recent CLEO measurements is also summarized in graphical form in Figs. 27 and 28.

A number of features of these decays were predicted in advance. For instance, Lipkin pointed out [96] that due to interference between the penguin diagrams shown in Fig. 19e and 19f, the rate for $B \to \eta K$ is suppressed and the rate for $B \to \eta' K$ is enhanced. Detailed predictions by Chau et al. [80] and subsequent authors show this pattern, but the predicted enhanced rate for $B \to \eta' K$ ($\sim$1–2×10^{-5}) was still far below the recently measured value. Gronau and Rosner suggested [34] the possibility that there could be significant enhancements to the rate for the decay $B \to \eta' K$ due to flavor-singlet (hairpin) amplitudes.

It is worthwhile commenting on the evolution of the theoretical predictions given in Tables 4 and 5. The basic method of using effective Hamiltonian theory has remained unchanged since the original Bauer, Stech and Wirbel [32] calculations in 1987. However there have been significant improvements in the detailed implementation: effective Wilson coefficients [97]; knowledge of the CKM matrix elements [99]; values of the relevant quark masses and quark mixing angles (especially important for η and η' decay channels); proper treatment of the QCD

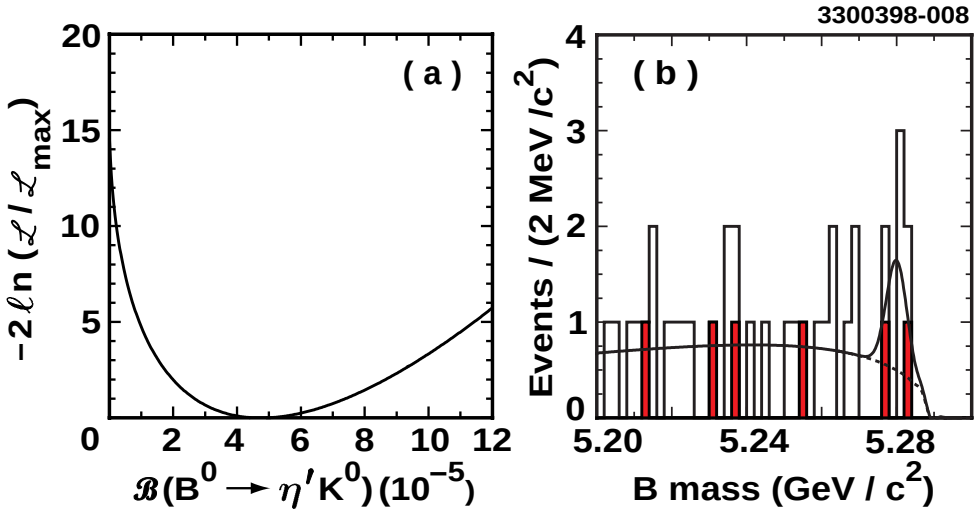

Figure 25: (a) $-2\ln\mathcal{L}/\mathcal{L}_{\rm max}$ and (b) mass projection plot for $B^0 \to \eta' K^0$, with curves the same as in Fig. 24. The histograms show submodes: $\eta' \to \eta\pi\pi$ with $\eta \to \gamma\gamma$ (shaded) and $\eta' \to \rho\gamma$ (open).

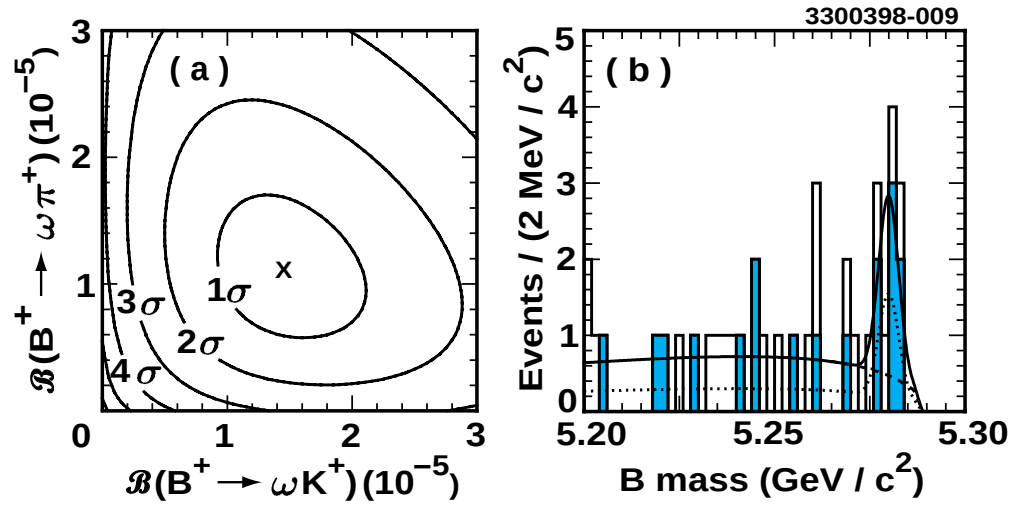

Figure 26: (a) Likelihood contours and (b) mass projection plot for $B^+ \to \omega h^+$. In (b), the curves are the same as for Fig. 24, with the addition of a dotted line showing the $B^+ \to \omega K^+$ component of the fit. The histograms show $B^+ \to \omega K^+$ (shaded) and $B^+ \to \omega\pi^+$ (open).

anomaly [98]; and more complete treatment of non-factorizable contributions using the empirical color factor ξ. Thus the newest predictions [81], epitomized by the recent comprehensive calculations of Ali, Kramer and Lü, represent a substantial advance over the older predictions [80]. In order to try to capture a sense of this progress, we have indicated the range of newer calculations with solid lines in Figs. 27 and 28, while the range of calculations prior to 1997 is indicated by a dashed line.

Several of the CLEO limits restrict the range of recent predictions, as indicated by bold face in the Tables 4 and 5 and overlap of the "X" and the theory line in Figs. 27 and 28. In other cases they are able to eliminate some theoretical hypotheses which have been advanced to account for the surprisingly large rate for $B \to \eta' K$. For instance the conjecture that the rate is enhanced by a substantial $c\bar{c}$ admixture in the η', i.e. η'-η_c mixing [100], appears unlikely. Such a mechanism would also yield a large rate for $B \to \eta' K^*$, in contradiction with the limit given in Table 4. Several authors [101] now agree that the $c\bar{c}$ admixture in the η' is small and actually leads to destructive interference, hence smaller rate, for values of the phenomenological parameter $\xi < 0.3$ (see Sec. 2.6), where the rate predictions are largest.

A typical range of predictions for the rate for $B \to \eta' K$ is (2–4)$\times 10^{-5}$ [26, 83]. Some theorists believe that the present experimental value is a fluctuation and will end up in this range [26], while others suggest that the rate can be enhanced by a variety of mechanisms: use of an even smaller value of the strange quark mass than is now being used [102]; use of somewhat larger values of form factors [102, 103]; use of smaller values of the CKM phases γ [84]; including non-factorizable contributions arising from the QCD anomaly [104, 105, 106], or modification to the Wilson coefficients whereby the value of the color-factor ξ is different for odd and even penguin coefficients [83]. In order to account for the $B \to \eta' K$ data, Deshpande et al. [84] used constructive interference for the $c\bar{c}$ admixture (now apparently ruled out) and the CKM phase $\gamma = 35°$; a recent fit [99] of all relevant data excludes this value: $\gamma = (64 \pm 12)°$. Further data should help distinguish among the various possibilities. The rate for $B \to \eta' K^*$ may prove to be crucial in this regard.

The situation for the ω and ϕ decays is quite unclear at present. There have been several recent theoretical papers specifically addressing vector-pseudoscalar final states [83, 84, 85, 108], with an emphasis on the $B^+ \to \omega K^+$, $B^+ \to \omega \pi^+$, $B^+ \to \phi K^+$, and $B \to \phi K^*$ decays, where there are measurements or good limits. The theoretical estimates for $B^+ \to \omega K^+$ [26, 84] tend to be $<10^{-5}$ except when $\xi \sim 0$ or $\xi > 0.5$. The decay $B^+ \to \phi K^+$ is closely related but there is as yet no evidence for this decay; the CLEO 90% CL limit of 0.5×10^{-5} tends to exclude the large ξ range. The recent paper of Ali et al. [85] suggests that these decays belong to a class where factorization may not work well (hence ξ may be different than it is for other decays), since the largest Wilson coefficients are not present in the amplitudes for these processes. Cheng and Tseng [83] come to similar conclusions for quite different reasons.

There have been a variety of other speculations regarding the rates for these charmless processes. Ciuchini et al. have suggested that there could be substantial enhancements in certain decays due to "charming penguins", where the charm-quark contribution in the loop becomes large due to large non-perturbative corrections to the effective-Hamiltonian calculations [107]. They predict that final states such as ρK, ϕK^*, ωK, and ωK^* would be substantially enhanced, though

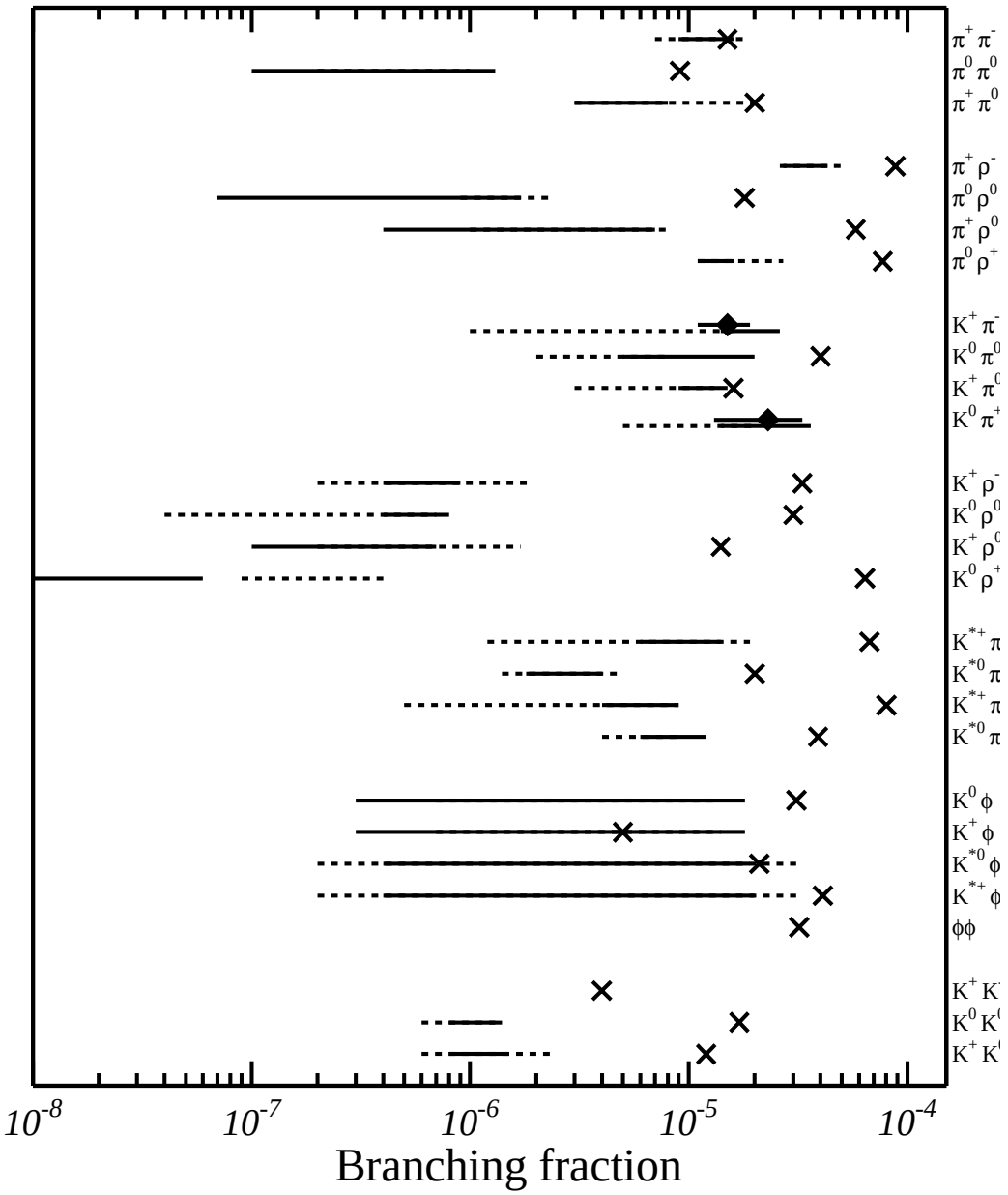

Figure 27: Graphical summary of various recent CLEO measurements of charmless hadronic B decays. Limits are denoted by "X", significant measurements by (diamond) points with error bars, and recent (pre-1997) theoretical ranges by solid (dashed) lines.

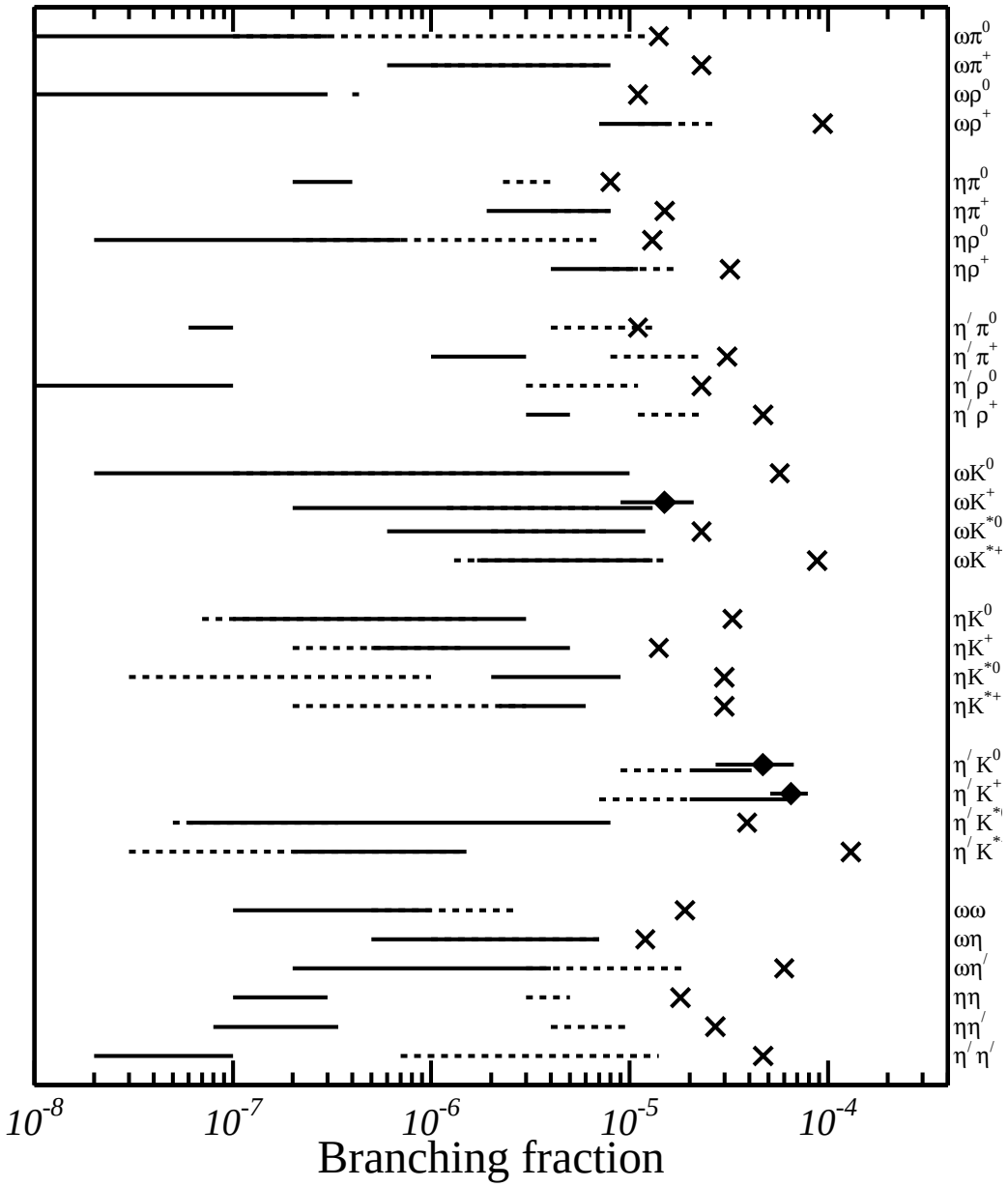

Figure 28: Same as the previous figure with modes involving η, η' and ω mesons.

even this model is unable to account for the large measured rate for $B^+ \to \omega K^+$. Some limits presented here, especially that for $B^+ \to K^0\rho^+$, tend to indicate that such enhancements are not huge.

5.2 Non-resonant decays

The processes discussed so far have been two-body or quasi-two-body decays. Results also have been reported for a variety of higher multiplicity, non-resonant decays. Such studies are important since it is not obvious how much of the final state $K\pi\pi$, for example, is $K^*\pi$, $K\rho$, non-resonant, or some other possibilities. Additional incentive for measuring such decays was provided by a paper [109] pointing out that interference effects in the 3π final state could lead to CP violation, and asymmetry measurements could potentially measure the weak phase γ. However, since this topic is unrelated to penguins, we do not discuss it further. The current experimental situation for these higher multiplicity decays is summarized in Table 6. In a few cases the limits are becoming restrictive but most are far away from the theoretically expected branching fractions. For instance the prediction for $B^+ \to 2\pi^+\pi^-$ is 10–50$\times 10^{-6}$ [109].

Table 6: Results from measurements of non-resonant B decay modes. We give the 90% confidence level upper limit on the branching fractions (UL $\mathcal{B}$). Modes above the line are expected to be dominated by penguins. Experiment key: AL (ALEPH [110]), AR (ARGUS [111]), C2 (CLEO II [112]), D (DELPHI [53]).

B^0 final state	Expt.	UL $\mathcal{B}$ (10^{-6})	B^+ final state	Expt.	UL $\mathcal{B}$ (10^{-6})
$K^+\pi^+2\pi^-$	D	230	$K^+\pi^+\pi^-$	C2	28
			$K^-\pi^+\pi^+$	C2	56
			$K^+K^+K^-$	C2	38
			$p\bar{p}K^+$	C2	89
$\bar{\Lambda}p\pi^-$	AR	180	$\bar{\Lambda}p\pi^+\pi^-$	AR	200
$\pi^+\pi^-\pi^0$	AR	720	$2\pi^+\pi^-$	C2	41
			$\pi^+2\pi^0$	AR	890
			$K^+K^-\pi^+$	C2	75
			$p\bar{p}\pi^+$	C2	53
$2\pi^+2\pi^-$	D	230	$2\pi^+\pi^-\pi^0$	AR	4000
$\pi^+\pi^-2\pi^0$	AR	3100			
$p\bar{p}\pi^+\pi^-$	AL	150			
$2\pi^+2\pi^-\pi^0$	AR	9000	$3\pi^+2\pi^-$	AL	280
			$p\bar{p}2\pi^+\pi^-$	AL	370
$3\pi^+3\pi^-$	AL	660	$3\pi^+2\pi^-\pi^0$	AR	6300
$3\pi^+3\pi^-\pi^0$	AR	11000			

5.3 Decays of B_s^0 mesons

There have been relatively few studies of the B_s^0 meson since the mass, 5370 MeV, is too large for production at the Υ(4S) resonance, so CLEO and ARGUS

Table 7: Results from measurements of B_s^0 decay modes. We give the 90% confidence level upper limit on the branching fractions (UL $\mathcal{B}$), and the range of theoretical predictions [27, 113].

B_s^0 decay mode	Experiment	UL $\mathcal{B}$ (10^{-6})	Theory (10^{-6})
K^+K^-	DELPHI[53]	46	3–21
$K^+\pi^-$	ALEPH[78]	210	10–18
$\pi^+\pi^-$	ALEPH[78]	170	
$p\bar{p}$	ALEPH[78]	59	
$\pi^0\pi^0$	L3[114]	210	
$\eta\pi^0$	L3[114]	1000	0.001–0.02
$\eta\eta$	L3[114]	1500	0.4–5.6

have not studied these decays. Thus all results for B_s^0 charmless hadronic decays are from the various LEP detectors. The physics is very similar for B_s^0 as for B_d^0 mesons; imagine the u or d spectator quark in Fig. 19 replaced by an s quark, with appropriate changes to the final state mesons. Thus the analogue of the penguin decay $B \to K\pi$ is $B_s^0 \to KK$. In Table 7, we summarize the present knowledge concerning rare B_s^0 decays. The limit for $B_s^0 \to K^+K^-$ is close to the expectation, but all others are not. However, new information on these decays can be expected in the future from hadronic colliders.

5.4 Inclusive decays

There have been a variety of inclusive searches for gluonic penguins, which typically involve final states with (hidden or open) strangeness. Inclusive decays are intriguing partly because direct CP violation might be observed as a difference between the numbers of positively and negatively charged kaons [115]. We describe several searches for inclusive decays, beginning with attempts to measure the inclusive $b \to sg^*$ rate and including one quite surprising observation.

Even though the gluonic penguin $b \to sg^*$ does not have a good signature, several experiments have used ingenuity to try to measure the inclusive process. The ARGUS collaboration searched for $b \to sg^*$ in samples where one B of a $B\bar{B}$ event is fully or partially reconstructed. They searched for decays of the other B involving a kaon and multiple pions, a typical signature of the $b \to sg^*$ process. They found two events where no possible sub-combination is consistent with any charmed particle and set a 90% CL upper limit of 8% on the branching fraction for $b \to sg^*$ [116].

DELPHI [117] looked for $b \to sg^*$ by searching for an excess of high p_t kaons, since more energy is available for kaons from $b \to s$ decays than from $b \to c \to s$ decays. A fit to the kaon p_t distribution provided a preliminary limit of $\mathcal{B}(b \to sg^*) < 5\%$ at 95% confidence level.

There have been two indirect searches for $b \to sg^*$. CLEO set an upper limit of 6.8% [118] by accounting for all other types of B decays. DELPHI [119] performs a similar search, and finds a limit of 4% at 90% confidence level [120]. While none of these searches is yet sufficiently sensitive to observe the $\sim 1\%$ signal expected from Standard Model processes, they appear to exclude models [38, 40, 41, 42]

where the rate is enhanced by an order of magnitude (see Sec. 2.8).

CLEO has searched [121] for a ϕ meson accompanied by an X_S system consisting of a charged or neutral K meson and zero to four pions, of which at most one can be a π^0. The X_S system was required to have a mass less than 2 GeV, corresponding to a ϕ meson momentum of $\sim$2.1 GeV/c; in this region the background is small for ϕ mesons arising from $b \to c$ processes, potentially allowing detection of a $b \to sg^*$ signal. CLEO observed no signal and, using the model of Deshpande et al. [122], they set an upper limit $\mathcal{B}(B \to \phi X_S) < 1.3 \times 10^{-4}$. The theoretical expectation for this process is $(0.6 - 2.0) \times 10^{-4}$ [122].

The only positive evidence for inclusive charmless hadronic B decays is from the CLEO analysis of the decay $B \to \eta' X_S$ [123]. The technique is the same as for the ϕ inclusive search except that the kaons were required to be charged. The momentum of η' mesons, reconstructed with the decay chain $\eta' \to \eta\pi^+\pi^-$, $\eta \to \gamma\gamma$, was required to be in the range $2.0 < p_{\eta'} < 2.7$ GeV/c in order to reduce background from $b \to c$ processes. The values of ΔE and M, as defined above, were required to satisfy $|\Delta E| < 0.1$ GeV and $M > 5.275$ GeV.

The η' mass distribution is shown in Fig. 29; a clear signal of 39 ± 10 events is seen for on-resonance data and none for the below-threshold sample. The signal, obtained by subtracting the scaled off-resonance data in bins of X_S mass, is plotted in Fig. 30. Note the four events corresponding to $B^+ \to \eta' K^+$ and the absence of events in the $K^*(892)$ mass region, both consistent with the exclusive results discussed in Sec. 5.1.3. Also shown in Fig. 30 are distributions for potential background modes such as $B \to D\eta'$ and $B \to D^*\eta'$. Though these also tend to have large X_S mass, they are more peaked than the data. These and other studies suggest that the observed signal does not arise primarily from color-suppressed $b \to c$ decays, though it is difficult to rule this out completely without better models of such processes. The efficiency was calculated assuming that the signal arises solely from gluonic penguin decays, with an equal admixture of X_S states from the kaon up to $K_4^*(2200)$. The efficiency of $(5.5 \pm 0.3)\%$ leads to $\mathcal{B}(B \to \eta' X_S) = (6.2 \pm 1.6 \pm 1.3) \times 10^{-4}$ for $2.0 < p_{\eta'} < 2.7$ GeV/c. The systematic error is dominated by the uncertainty in the X_S modeling.

Many theorists suggest that the $B \to \eta' X_S$ result is the most surprising of those included in this review — the theoretical expectation for the high-momentum η' branching fraction is $\sim 1 \times 10^{-4}$. Atwood and Soni [104] first suggested that the very large rate could be due to the QCD anomaly via $b \to sg^* \to s\eta' g$. Later Fritzsch [124] suggested a similar anomaly-mediated $b \to sg$ process. Both processes have a hard X_S mass spectrum in rough agreement with that shown in Fig. 30, but Fritzsch's 2-body process would be falling by 2.5 GeV, while the 3-body decay of Atwood and Soni would still be rising. There have been several other recent papers discussing $B \to \eta' X_S$ [102, 103, 125, 126]. They consider the anomaly and the possibility of non-SM contributions. It is still not clear whether one of these anomaly models can quantitatively account for the $B \to \eta' X_S$ result, though there don't seem to be any better explanations at present without invoking new physics. Since other inclusive processes such as $B \to \phi X_S$ are not enhanced, it seems likely that this result is indeed an "anomaly" involving the η' meson.

In a similar search for high-momentum η mesons, CLEO finds no evidence for a signal and sets a 90% CL upper limit for the branching fraction of 4.4×10^{-4}. The theoretical expectation is that the rate for η mesons would be suppressed relative by about an order of magnitude since their flavor-singlet component is small.

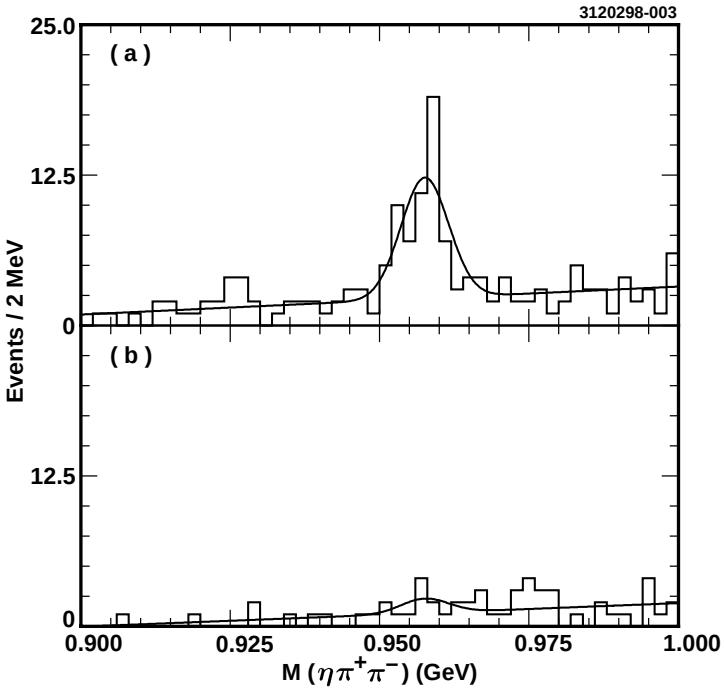

Figure 29: The η' mass distribution for (a) on-resonance and (b) below-threshold data.

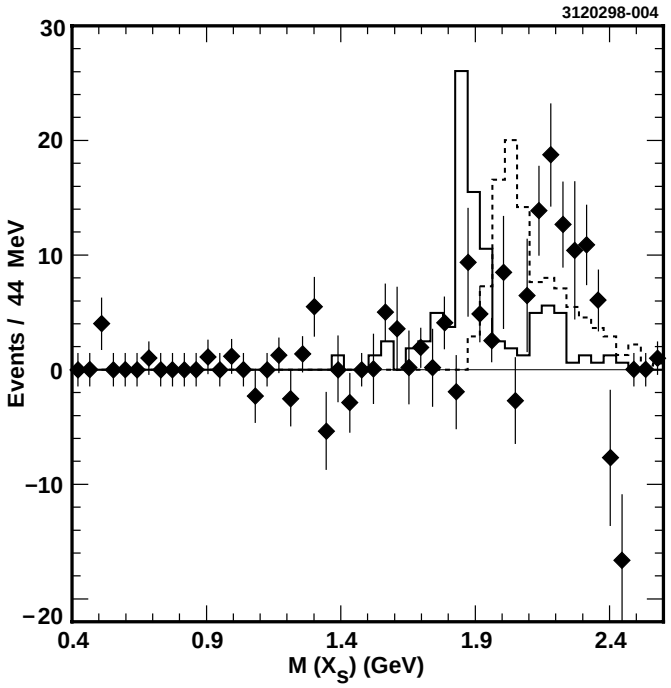

Figure 30: Distribution of X_S mass for data (points with error bars) and possible backgrounds: $B \to D\eta'$ (solid histogram) and $B \to D^*\eta'$ (dashed histogram). The normalization of the backgrounds is arbitrary.

6 FUTURE PROSPECTS

Table 8: Comparison of future B experiments. Parameters which do not change between different experiments at the same collider are entered only once.

Expt.	Collider	Beams	$\sqrt{s}$ (GeV)	Year online	$\mathcal{L}$ (10^{33} cm^{-1} s^{-1})	$\sigma(b\bar{b})$ (nb)	$b\bar{b}$ pairs (10^7/yr)	$\beta\gamma c\tau$ (μm)	$\sigma(b\bar{b})$ $/\sigma(q\bar{q})$
CLEO III	CESR	e^+e^-	10	1999	1.2	1	1.2	30	$3 \cdot 10^{-1}$
	CESR-IV		10	?	30	1	30	30	$3 \cdot 10^{-1}$
BaBar	PEP-II	e^+e^- †	10	1999	3-10	1	3-10	270	$3 \cdot 10^{-1}$
Belle	KEK-B	e^+e^- †	10	1999	3-10	1	3-10	200	$3 \cdot 10^{-1}$
HERA-B	HERA	pN	40	1998	—	6-12	50-100	9000	$1 \cdot 10^{-6}$
CDF II	Tevatron	$p\bar{p}$	1800	2000	0.2-1.0	100000	20000	500	$1 \cdot 10^{-3}$
D0									
BTeV ‡				2004	0.2			5000	
LHC-B ‡	LHC	pp	14000	2005	0.15	500000	75000	7000	$5 \cdot 10^{-3}$
Atlas								500	
CMS									

† Asymmetric beam energies. ‡ Forward detector.

Future measurements require more produced B mesons and good background rejection. The CLEO II experiment has a substantial amount of new data in the analysis pipeline (see Table 1) and continues to accumulate even more statistics. There are a variety of new experiments poised to do rare-B physics in the near and longer term as summarized in Table 8.

The CESR machine will be upgraded to higher luminosity and the CLEO detector will get a particle identification device and a new tracking system (CLEO III detector [127]). Also under construction are two new $\Upsilon(4S)$ colliders, the Positron-Electron Project-II (PEP-II) at the Stanford Linear Accelerator Center (SLAC) with the BaBar [128] experiment and KEK-B at the high energy laboratory in Japan with the Belle experiment [129]. These new machines have asymmetric beam energies for indirect CP violation measurements, which will also help background suppression because of the detached B vertex (see the $\beta\gamma c\tau$ column in Table 8). All "B Factory" experiments (BaBar, Belle, CLEO III) are expected to come online in 1999. They should be able to reach branching fractions of $\mathcal{O}(10^{-7})$ at the design luminosity. Unlike CESR, the new colliders have a double ring structure, thus in principle, they offer better potential for higher luminosity. There are some ideas of how to convert CESR into a double ring symmetric collider (CESR IV) for luminosity upgrades beyond the CLEO III phase [130].

The clean experimental environment at e^+e^- colliders is ideal for background suppression when looking for penguin processes which have very small branching fractions. Unfortunately, the $e^+e^- \to b\bar{b}$ cross-section is only 1 nb, making it very difficult to reach extremely rare decay modes. Hadronic colliders, with $b\bar{b}$ cross-sections approaching 1 mb, may offer the ultimate experimental avenue to the secrets of B physics. On the other hand, the total cross-section at hadronic colliders is much larger, making background rejection the dominant experimental obstacle. The detector recording rate is limited by technological constraints. B

data can easily be lost by the inability of an experiment to reduce background rates to manageable recording rates. It should be emphasized that hadronic colliders are built with the primary goal of studying ultra-high-energy processes which produce particles with large transverse momenta to the beam (P_t). In contrast, B decays produce particles with transverse momenta not much higher than ordinary beam interactions. So far, high-P_t detectors at the Tevatron (CDF and D0) have been able to trigger on B physics only in di-muon modes. Since off-line background suppression has been accomplished by detached B vertex cuts, inclusion of a detached vertex requirement in the trigger may be the best triggering strategy for non-leptonic rare decays.

There have been some dedicated experiments to study c and b quark physics with hadronic beams in fixed-target mode in which a hadronic beam (π^- or p) collides with a stationary nuclear target (N). While the fixed target charm program has played a complementary role to $e^+e^- \to c\bar{c}$ studies, the fixed target experiments barely succeeded in observing some inclusive signals from tree-level $b \to c$ decays of b quarks [131]. Since most of the incident beam energy is wasted providing the motion of the center-of-mass, the effective collision energy was rather low resulting in a very small $b\bar{b}$ cross-section. To compound these experimental difficulties, all beam and target fragments entered the detection apparatus together with B decay products. The latest attempt to study B physics in fixed target mode is represented by the HERA-B experiment [132] which will collide the proton beam from the Hadron-Electron Ring Accelerator facility (HERA) at DESY with a wire target inserted into the beam pipe. Use of modern technologies offers hope for success, though as in the previous fixed target experiments, the HERA-B experiment will have to contend with cross sections as low as in e^+e^- colliders and with hadronic backgrounds as high as in $p\bar{p}$ colliders. The first run is foreseen for 1998, with a full capacity run in 1999.

The Tevatron collider is in the midst of an upgrade program with turn-on planned for 2000. Luminosity will be substantially increased, with further luminosity upgrades possible in the long term future ("TeV33"). Improved vertex detectors in CDF-II [133, 134] and the D0 upgrade [135, 134] will help background suppression. The D0 experiment will acquire a magnetic field, but the tracking system will remain very compact. CDF-II will implement a $B \to h^+h^-$ trigger. Unfortunately, even if this trigger is successful, CDF-II will have difficulty distinguishing $B^0 \to \pi^+\pi^-$ from $B^0 \to K^+\pi^-$ and $B_s^0 \to K^+K^-$ because of the lack of high momentum particle identification.

In the farther future (2005), the LEP tunnel will house a new pp collider, the Large Hadron Collider (LHC), with high P_t experiments ATLAS [136] and CMS [137]. The larger center-of-mass energy will increase the $b\bar{b}$ cross-section and improve the signal-to-background ratio. Since the event rate at the LHC design luminosity will be too high to record $b\bar{b}$ data, the B physics program in these high P_t experiments may be limited to initial lower luminosity running.

Both the Tevatron and LHC programs contemplate installation of dedicated b experiments (BTeV [138] and LHC-B [139]). The machine luminosity would be reduced for these experiments to keep data rates at manageable levels. Without the constraints of high P_t physics, the detectors can be optimized for b physics. Both detectors would operate in the forward rather than the central region. Forward detector geometry offers enough space for efficient particle identification in the entire momentum range (see below). Furthermore, the decay length of B mesons is longer than it is in the central region, allowing for better background

suppression in the off-line analysis and in the trigger. Last but not least, the entire trigger bandwidth can be saturated with b physics events.

Improvement in particle identification is also crucial at e^+e^- machines. The separation of gluonic $b \to s$ penguin decays from tree-level $b \to u$ decays is already marginal for CLEO II (Sec. 5.1.2) and there are more ambitious goals. We would like to have measurements of $b \to d$ penguin decays despite large backgrounds from the dominant $b \to s$ decay; measurement of the electroweak penguin $B^+ \to \phi\pi^+$ with a large $B^0 \to \phi K^+$ background will be a tremendous challenge. The BaBar experiment will use a Detector of Internally Reflected Čerenkov (DIRC) to measure the Čerenkov angle of light from particles traversing quartz bars. The DIRC gives at least 2.5σ π-K separation up to the maximum momentum of 4 GeV. The Belle experiment uses an aerogel threshold Čerenkov detector to identify kaons with an 8% misidentification rate for momenta between 1 and 3 GeV. The CLEO III detector will use a Ring Imaging Čerenkov (RICH) detector with a solid radiator to achieve 4σ π-K separation at a momentum of 2.6 GeV/c, the maximum value from B decays. HERA-B will have a gaseous RICH detector, which is expected to provide 90% efficient kaon identification with less than 2% misidentification background. CDF-II and D0 are limited to kinematic separation of kaons and pions, with little additional help from dE/dx. The BTeV and LHC-B designs include gaseous RICH detectors.

7 CONCLUSIONS

The penguin program already has been a profitable one, but much penguin physics is still left to be done. The measured $b \to s\gamma$ rate has been found to be consistent with Standard Model predictions and has provided interesting constraints on new physics models. Since these measurements are still statistics limited, more data will provide improved constraints and even allow measurement of $|V_{td}|$ from $b \to d\gamma$ penguin decays.

Limits on the rates of electroweak penguins $b \to s\ell^+\ell^-$ and vertical penguins such as $b \to \ell^+\ell^-$ are currently orders of magnitude above the predictions of the Standard Model and give no evidence for non-SM effects. These processes need to be measured to confirm Standard Model predictions or to distinguish between different types of new physics. Some penguin modes such as $b \to s\nu\bar{\nu}$ or $B^0 \to \gamma\gamma$ will be very difficult to observe, since they are not suitable for detection at hadronic colliders and the e^+e^- machines are likely to be limited by the $b\bar{b}$ statistics.

Several suspected gluonic penguins have been observed. The $B \to K\pi$ rates are consistent with theoretical predictions. However, the $B \to \omega K$, $B \to \eta' K$ and $B \to \eta' X_s$ rates are all surprisingly large! These rates have stimulated many Standard Model and non-SM ideas and more data are needed to resolve the situation. More work needs to be done to separate the gluonic penguin amplitudes from electroweak penguin or $b \to u$ amplitudes in hadronic decays. The rates of penguin decays such as $B \to K\pi$, $B^0 \to \phi K^0_S$ and $B^0 \to \eta' K^0_S$ must be measured precisely to give us insight into CP violation. The measurement of many penguin modes is needed to give us a handle on penguin pollution in indirect CP violation.

The outlook for penguins is very promising. Within the next five years we should have good handles on most electromagnetic and gluonic penguin modes,

and perhaps a beginning of an understanding of suppressed modes which are dominated by electroweak penguins or annihilation diagrams. Perhaps there can be a reunion in the year 2002 on the 25th birthday of the penguin and we can look back at the tremendous progress that has been made! Darts anyone?

ACKNOWLEDGMENTS

The authors would like to thank A. Ali, H-Y. Cheng, S. Oh, and A. Soni for useful discussions. We also thank Ahmed Ali, Bill Ford, and Amarjit Soni for their careful reading of the manuscript. We acknowledge our colleagues on CLEO, ARGUS, ALEPH, DELPHI, L3, CDF, and D0 for their contributions to the experimental work in this review. This review was supported by the U.S. Department of Energy.

Literature Cited

1. Cabibbo N. *Phys. Rev. Lett.* 10:531 (1963); Kobayashi M, Maskawa T. *Prog. Theor. Phys.* 49:652 (1973)
2. Wolfenstein L. *Phys. Rev. Lett.* 51:1945 (1983)
3. Ellis J, et al. *Nucl. Phys.* B131:285-307 (1977)
4. This account has been reconstructed, not from the pervasive rumor mill, but with the help of Melissa Franklin and an account by John Ellis in Shifman's introduction to "ITEP Lectures in Particle Physics", published by World Scientific (hep-ph/9510397).
5. Vainshtein AI, Zakharov VI, Shifman MA. *JETP Lett.* 22:55-56 (1975); Shifman MA, Vainshtein AI, Zakharov VI. *Nucl. Phys.* B120:316 (1977)
6. Guberina B, Peccei RD, Rückl R. *Phys. Lett.* 90B:169 (1980)
7. Bander M, Silverman D, Soni A. *Phys. Rev. Lett.* 43:242 (1979)
8. Eilam G. *Phys. Rev. Lett.* 49:1478 (1982)
9. Bertolini S, Borzumati F, Masiero A. *Phys. Rev. Lett.* 59:180 (1987); Deshpande NG, et al.. *Phys. Rev. Lett.* 59:184 (1987); Grinstein B, Springer R, Wise M. *Phys. Lett.* B202:138 (1988)
10. Hou W-S, Soni A, Steger H. *Phys. Rev. Lett.* 59:1521 (1987); Hou W-S. *Nucl. Phys.* B308:561 (1988)
11. Lenz A, Nierste U, Ostermaier G. *Phys. Rev.* D56, 7228 (1997)
12. Detailed discussion of the status of the theoretical calculations for $b \to s\,\gamma$ can be found in Ref. [13]. See also: Greub C, Hurth T, *Phys. Rev.* D56:2934 (1997); Buras AJ, Kwiatkowski A, Pott N, *Phys. Lett.* B414:157 (1997); and Refs. [14] and [15]
13. Ali A. Report No. DESY 97-102, hep-ph/9709507, to be published in *Proc. 7th International Symposium on Heavy Flavor Physics* (1997)
14. Ciuchini M, Degrassi G, Gambino P, Giudice GF. Report No. CERN-TH/97-279, hep-ph/9710335 (1997); see also Ciafaloni P, Romanino A, Strumia A. Report No. IFUP-TH 48/97, hep-ph/9710312 (1997)
15. Chetyrkin K, Misiak M, Münz M. *Phys. Lett.* B400:206 (1997)
16. The numbers in the braces given below are the predictions for the R_{K^*} ratio in percent. Deshpande NG, et al. *Phys. Rev. Lett.* 59:183 (1987) {6}; Dominquez CA, et al. *Phys. Lett.* B214:459 (1988) $\{28 \pm 11\}$; Altomari T. *Phys. Rev.* D37:3 (1988) {4.5}; Deshpande NG, Trampetić J. *Mod. Phys. Lett.* A4:2095 (1989) $\{6 - 14\}$; Aliev TM, et al. *Phys. Lett.* B237:569 (1990) {39}; Ali A, Greub C. *Phys. Lett.* B259:182 (1991) $\{13 \pm 3\}$; Faustov RN, Galkin VO. *Mod. Phys. Lett.* A7:2111 (1992) {6.5}; Ali A, Ohl T, Mannel T. *Phys. Rev.* 298B:195 (1993) $\{3.5-12.2\}$; El-Hassan E, Riazuddin. *Phys. Rev.* D47:1026 (1993) $\{0.7-12\}$; O'Donnell J, Tung HK. *Phys. Rev.* D48:2145 (1993) {10}; Ball P. Report No. TUM-T31-43/93, hep-ph/9308244 (1993) $\{20 \pm 6\}$; Colangelo P, et al. *Phys. Lett.* B317:183 (1993) $\{17 \pm 5\}$; Ali A, Braun VM, Simma H. *Z. Phys.* C63:437 (1994) $\{16 \pm 5\}$; Bernard C, Hsieh P, Soni A. *Phys. Rev. Lett.* 72:1402 (1994) $\{6.0 \pm 1.1 \pm 3.4\}$; Narison S. *Phys. Lett.* B327:354 (1994) $\{15 \pm 4\}$; Atwood S, Soni A. *Z. Phys.* C64:241 (1994) $\{1.6 - 2.5\}$; Ciuchini M, et

al. *Phys. Lett.* B334:137 (1994) $\{23 \pm 9\}$; Ref. [17] $\{28 - 40\}$; Ref. [18] $\{16 \pm 5\}$; Ref. [19] $\{16^{+4}_{-3}\}$
17. Ali A, Mannel T. *Phys. Lett.* B264:447 (1991)
18. Ali A, Braun VM, Simma H. *Z. Phys.* C63:437 (1994)
19. Del Debbio L, Flynn JM, Lellouch L, Nieves J (UKQCD Collaboration). *Phys. Lett.* B416:392 (1998)
20. Ali A, Hiller G, Handoko LT, Morozumi T. *Phys. Rev.* D55:4105 (1997); See also Refs. [13, 21]
21. Buras AJ. *Proc. 28th International Conference on High Energy Physics*, Warsaw, Poland, pp. 243-270 (1996)
22. Okubo S. *Phys. Lett.* 5, 165 (1963); Zweig G. Report No. CERN-TH-412 (1964); Iizuka I. *Prog. Theor. Phys. Suppl.* 37:21 (1966)
23. For a simple introduction to the effective theory of penguin decays see e.g. Buras AJ. *Acta Phys. Polon.* B26:755 (1995) and Ref. [24]. For historical development of the theory see: Wilson KG. *Phys. Rev.* 179:1499 (1969); Altarelli G, Maiani L. *Phys. Lett.* B52:351 (1974); Gaillard MK, Lee BW. *Phy. Rev. Lett.* 33:108 (1974); Altarelli G, Curci G, Martinelli G, Petrarca S. *Phys. Lett.* B99:141 (1981); *Nucl. Phys.* B187:461; Buras AJ, Weisz PH. *Nucl. Phys.* B333:66 (1990); Buras AJ, et al. *Nucl. Phys.* B370:69 (1992); and Ref. [15]
24. Falk AF. *Proc. International Symposium on Vector Boson Self-interactions*, Los Angeles, CA, pp. 136-147 (1995)
25. Chay J, Georgi H, Grinstein B. *Phys. Lett.* B247:399 (1990)
26. Ali A, Greub C. *Phys. Rev.* D57:2996 (1998)
27. Deandrea A, et al. *Phys. Lett.* B318:549 (1993); B320:170 (1994)
28. Kramer G, Palmer WF, Simma H. *Nucl. Phys.* B428:77 (1994); *Z. Phys.* C66:429 (1995)
29. Feynman RP in *Symmetries in Particle Physics*, ed. Zichichi A, Acad. Press, p.167 (1965); Haan O, Stech B. *Nucl. Phys.* B22:448 (1970)
30. Bjorken JD in *New Developments in High-Energy Physics*, ed. Floratos EG, Verganelakis A *Nucl. Phys.* (Proc. Suppl.) 11:321 (1989)
31. Browder TE, Honscheid K, Pedrini D. *Ann. Rev. Nucl. Part. Sci.* 46:395 (1996)
32. Bauer M, Stech B. *Phys. Lett.* B152:380 (1985); Bauer M, Stech B, Wirbel M. *Z. Phys.* C34:103 (1987); Neubert M, Rieckert V, Xu QP, Stech B in *Heavy Flavours*, ed. Buras AJ, Lindner H, World Scientific, Singapore (1992); Cheng HY. *Phys. Lett.* B335:428 (1994); Soares JM. *Phys. Rev.* D51:3518 (1995)
33. Fleischer R. *Phys. Lett.* B365:399 (1996); Gronau M, Rosner JL. *Phys. Rev. Lett* 76:1200 (1996); Dighe AS, Gronau M, Rosner JL. *Phys. Rev.* D54:3309 (1996); *Phys. Rev.* D54:4677 (1996); Ref. [34]
34. Gronau M, Rosner JL. *Phys. Rev.* D53:2516 (1996); Dighe AS, Gronau M, Rosner JL. *Phys. Lett.* B367:357 (1996); Dighe AS. *Phys. Rev.* D54:2067 (1996)
35. London D, Peccei RD. *Phys. Lett.* B223:257 (1989)
36. London D, Soni A. *Phys. Lett.* B407:61 (1997)
37. For an excellent review, see Gronau M, London D. *Phys. Rev.* D55:2845 (1997) and references therein.
38. Kagan AL. *Phys. Rev.* D51:6196 (1995); Ciuchini M, Gabrielli E, Giudice GF. *Phys. Lett.* B388:353 (1996)
39. Aliev TM, Dobroliubov MI. *Phys. Lett.* B237:573 (1990)
40. Grzadkowski B, Hou W-S. *Phys. Lett.* B272:283 (1991)
41. Kagan AL, Rathsman J. Report No. hep-ph/9701300 (1997)
42. Hou W-S, Tseng B. *Phys. Rev. Lett.* 80:434 (1998)
43. Richman JD (Particle Data Group). *Phys. Rev.* D54:482 (1996)
44. Altarelli G, Petrarca S. *Phys. Lett.* B261:303 (1991); Bigi II, Blok B, Shifman MA, Vainshtein A. *Phys. Lett.* B323:408 (1994); Falk AF, Wise MB, Dunietz I. *Phys. Rev.* D51:1183 (1995); Bagan E, Ball P, Braun VM, Gosdzinsky P. *Nucl. Phys.* B432:3 (1994); *Phys. Lett.* B342:362 (1995); Bagan E, Ball P, Fiol B, Gosdzinsky P. *Phys. Lett.* B351:546 (1995); Voloshin MB. *Phys. Rev.* D51:3948 (1995); Dunietz I. *Phys. Rev.* D52:3048 (1995)
45. Honscheid K (Particle Data Group). *Phys. Rev.* D54:477 (1996)
46. Ammar R, et al. (CLEO Collaboration). *Phys. Rev. Lett.* 71:674 (1993)
47. Ammar R, et al. (CLEO Collaboration). Report No. CLEO CONF 96-05, contributed paper to *The 28th International Conference on High Energy Physics*, Warsaw, Poland (1996)
48. Deshpande NG, et al. *Phys. Lett.* B214:467 (1988); Colangelo P, et al. *Z. Phys.* C45:575

(1990)
49. Litke AM (ALEPH Collaboration). *Proc. 27th International Conference on High Energy Physics*, Glasgow, Scotland, p. 1333 (1994)
50. Alam MS, et al. (CLEO Collaboration). *Phys. Rev. Lett.* 74:2885 (1995)
51. Ali A, Greub C. *Phys. Lett.* B361:146 (1995)
52. Barate et al. (ALEPH Collaboration), Report No. CERN-EP/98-044 (1998) To be published in *Phys. Lett. B.*
53. Adam W, et al. (DELPHI Collaboration). *Z. Phys.* C72:207 (1996)
54. Adriani O, et al. (L3 Collaboration). *Phys. Lett.* B317:637 (1993)
55. Tartarelli GF, et al. (CDF Collaboration). Report No. FERMILAB-CONF-97-401-E (1997), contributed paper to International Europhysics Conference on High-Energy Physics (HEP 97), Jerusalem, Israel (1997)
56. Feindt M, Presented at *International Europhysics Conference on High-Energy Physics (HEP 97)*, Jerusalem, Israel (1997), Report No. hep-ph/9802380 (1998).
57. Chia S. *Phys. Lett.* B240:465 (1990); Peterson K. *Phys. Lett.* B282:207 (1992); Rizzo T. *Phys. Lett.* B315:471 (1993); He X, McKellar B. *Phys. Lett.* B320:165 (1994)
58. Abachi S, et al. (D0 Collaboration) *Phys. Rev. Lett.* 78:3634 (1997)
59. Bertolini S, et al. *Nucl. Phys.* B294:321 (1987); Okada Y. *Phys. Lett.* B315:119 (1993); Garisto R, Ng JN. *Phys. Lett.* B315:372 (1993)
60. Hewett J, Wells JD. *Phys. Rev.* D55:5549 (1997)
61. Hewett J. Report No. hep-ph/9803370 (1998), to be published in *Proc. 7th International Symposium on Heavy Flavor Physics*, University of California, Santa Barbara
62. Ali A, Asatrian H, Greub C. Report No. DESY-97-255, hep-ph/9803314 (1998)
63. Atwood D, Blok B, Soni A. *Int. J. Mod. Phys.* A11:3743 (1996).
64. Abe F, et al. (CDF Collaboration). *Phys. Rev. Lett.* 76:4675 (1996)
65. Glenn S, et al. (CLEO Collaboration). *Phys. Rev. Lett.* 80:2289 (1998)
66. Albajar C, et al. (UA1 Collaboration). *Phys. Lett.* B262:163 (1991)
67. Abbott B, et al. (D0 Collaboration). Report No. FERMILAB-PUB-98-033-E, hep-ex/9801027 (1998), submitted to *Phys. Lett.* B
68. The ALEPH Collaboration, Report No. PA10-019, contributed paper to *The 28th International Conference on High Energy Physics*, Warsaw, Poland (1996)
69. Grossman Y, Ligeti Z, Nardi E. *Nucl. Phys.* B465:369 (1996); *Nucl. Phys.* B480:753 (1996)
70. Ali A. *Nucl. Phys. Proc. Suppl.* 59:86 (1997)
71. Chang HV, Lin GL, Yao YP. *Phys. Lett.* B415:395 (1997); Reina L, Ricciardi G, Soni A. *Phys. Rev.* D56:5805 (1997); Hiller G, Iltan EO. *Phys. Lett.* B409:425 (1997)
72. Acciarri M, et al. (L3 Collaboration). *Phys. Lett.* B363:137 (1995)
73. Ammar R, et al. (CLEO Collaboration). *Phys. Rev.* D49:5701 (1994)
74. Abe F, et al. (CDF Collaboration). *Phys. Rev.* D57:3811 (1997)
75. Acciarri M, et al. (L3 Collaboration). *Phys. Lett.* B391:474-480 (1997)
76. Battle M, et al. (CLEO Collaboration). *Phys. Rev. Lett.* 71:3922 (1993)
77. Asner DM, et al. (CLEO Collaboration). *Phys. Rev.* D53:1039 (1996); Anastassov A et al. (CLEO Collaboration). Report No. CLEO CONF 97-24, EPS-448, contributed paper to International Europhysics Conference on High-Energy Physics (HEP 97), Jerusalem, Israel (1997)
78. Buskulic D, et al. (ALEPH Collaboration). *Phys. Lett.* B384:471 (1996)
79. Godang R, et al. (CLEO Collaboration). *Phys. Rev. Lett.* 80:3456 (1998)
80. Publications submitted prior to the 1997 experimental results include Refs. [27, 28] and: Deshpande NG, Trampetić J. *Phys. Rev.* D41:895 (1990); Chau L-L, et al. *Phys. Rev.* D43:2176 (1991); 1998 erratum to be published; Simma H, Wyler, D. *Phys. Lett.* B272:395 (1991); Fleischer R. *Z. Phys.* C58:483 (1993); Du D-S, Xing Z. *Phys. Lett.* B312:199 (1993); *Z. Phys.* C62:81 (1994); *Phys. Lett.* B321:259 (1994); Davies AJ, Hayashi T, Matsuda M, Tanimoto M. *Phys. Rev.* D49:5882 (1994); Kramer G, Palmer WF. *Phys. Rev.* D52:6411 (1995); Du D-S, Guo L. *Z. Phys.* C75:9 (1997); Ebert D, Faustov RN, Galkin VO. *Phys. Rev.* D56:312 (1997)
81. New comprehensive calculations include Refs. [83, 84, 85].
82. Predictions for modes involving baryons: Deshpande NG, Trampetić J, Soni A. *Mod. Phys. Lett.* 3A:749 (1988); Chernyak VL, Zhitnitsky A. *Nucl. Phys.* B345:137 (1990); Jarfi M, et al. *Phys. Rev.* D43:1599 (1991)
83. Cheng H-Y, Tseng B. *Phys. Lett.* B415:263 (1997); Cheng H-Y, Tseng B. Report No. IP-

ASTP-01-98, hep-ph/9803457 (1998)
84. Deshpande NG, Dutta B, Oh S. *Phys. Rev.* D57:5723 (1998); Report No. OITS-644, hep-ph/9712445 (1997)
85. Ali A, Kramer G, Lü C-D. Report No. DESY 98-041, hep-ph/9804363 (1998); see also Ref. [26]
86. Albrecht H, et al. (ARGUS Collaboration). *Phys. Lett.* B254:288 (1991)
87. Avery P, et al. (CLEO Collaboration). *Phys. Lett.* B223:470 (1989)
88. Behrens BH, et al. (CLEO Collaboration). *Phys. Rev. Lett.* 80:3710 (1998)
89. Bergfeld T, et al. (CLEO Collaboration). Report No. CLNS 97/1537, hep-ex/9803018 (1997), submitted to *Phys. Rev. Lett.*
90. Albrecht H, et al. (ARGUS Collaboration). *Phys. Lett.* B241:278 (1990)
91. Bortoletto A, et al. (CLEO Collaboration). *Phys. Rev. Lett.* 62:2436 (1989)
92. Fleischer R, Mannel T. *Phys. Rev.* D57:2752 (1998)
93. Fleischer R, Mannel T. Report No. TTP97-22, hep-ph/9706261 (1997)
94. Gronau M, Rosner JL. Report No. CALT-68-2142, hep-ph/9711246 (1997), submitted to *Phys. Rev. D*
95. Buras AJ, Fleischer R, Mannel T. Report No. CERN-TH/97-307, hep-ph/9711262 (1997); Gérard J-M, Weyers J. Report No. UCL-IPT-97-18, hep-ph/9711469; Falk AF, Kagan AL, Nir Y, Petrov AA. *Phys. Rev.* D57:4290 (1997); Neubert M. Report No. CERN-TH/97-342, hep-ph/9712224 (1997); Atwood D, Soni A. Report No. AMES-HET 97-10, hep-ph/9712287 (1997), submitted to *Phys. Lett. B*; Fleischer R. Report No. CERN-TH/98-60, hep-ph/9802433 (1998)
96. Lipkin HJ. *Phys. Lett.* B254:247 (1991)
97. See for instance Buchalla G, Buras AJ, Lautenbacher ME. *Rev. Mod. Phys.* 68:1125 (1996)
98. Ali A, Chay J, Greub C, Ko P. Report No. DESY 97-235, hep-ph/9712372 (1997)
99. Parodi F, Roudeau P, Stocchi A. Report No. hep-ph/9802289
100. Halperin I, Zhitnitsky A. *Phys. Rev.* D56:7247 (1997); *Phys. Rev. Lett.* 80:438 (1998)
101. See Ref. [26, 98] and Feldmann Th, Kroll P, Stech B. Report No. WU B 98-2, hep-ph/9802409 (1998); Araki F, Musakhanov M, Toki H. Report No. hep-ph/9803356 (1998)
102. Kagan A, Petrov A. Report No. UCHEP-27, hep-ph/9707354 (1997)
103. Datta A, He X-G, Pakvasa S. Report No. UH-511-864-97, hep-ph/9707259 (1997)
104. Atwood D, Soni A. *Phys. Lett.* B405:150 (1997)
105. Ahmady MR, Kou E, Sugamoto A. Report No. RIKEN-AF-NP-274, hep-ph/9710509 (1997)
106. Du D-S, Kim CS, Yang Y-D. Report No. BIHEP-TH/97-15, hep-ph/9711428 (1997)
107. Ciuchini M, et al. *Nucl. Phys.* B512:3 (1998)
108. Dighe AS, Gronau M, Rosner JL. *Phys. Rev.* D57:1783 (1998)
109. Deshpande NG, Eilam G, He X-G, Trampetić J. *Phys. Rev.* D52:5354 (1995)
110. Benchouk C, Trabelsi K, et al. (ALEPH Collaboration). Report No. ALEPH 96-105, contributed paper to *The 28th International Conference on High Energy Physics*, Warsaw, Poland (1996)
111. Albrecht H, et al. (ARGUS Collaboration). *Phys. Lett.* B209:119 (1988)
112. Bergfeld T, et al. (CLEO Collaboration). *Phys. Rev. Lett.* 77:4503 (1996)
113. Du D-S, Xing Z. *Phys. Rev.* D48:3400 (1993)
114. Acciarri M, et al. (L3 Collaboration). *Phys. Lett.* B363:127 (1995)
115. Browder T, Datta A, He X-G, Pakvasa S. Report No. UH-511-864-96, hep-ph/9705320 (1997)
116. Albrecht H, et al. (ARGUS Collaboration). *Phys. Lett.* B353:554 (1995)
117. Battaglia M, Kluit PM (DELPHI collaboration). Report No. EPS-448, contributed paper to International Europhysics Conference on High-Energy Physics (HEP 97), Jerusalem, Israel (1997)
118. Coan TE, et al. (CLEO Collaboration). *Phys. Rev. Lett.* 80:1150 (1998)
119. Abreu P, et al. (DELPHI Collaboration). Report No. CERN-EP/98-07 (1998), to be published in *Phys. Lett. B*
120. Battaglia M, Kluit PM. Private communication. Ref. [119] actually quotes a limit on the non-standard model contributions to $b \to sg^*$, whereas we quote DELPHI's limit on the total $b \to sg^*$ rate
121. Edwards KW, et al. (CLEO Collaboration). Report No. CLEO-CONF-95-8, EPS0162, contributed paper to *EPS conference*, Brussels, Belgium (1995)

122. Deshpande NG, Eilam G, He X-G, Trampetić J. *Phys. Lett.* B366:300 (1996)
123. Browder TE, et al. (CLEO Collaboration). Report No. CLNS 98/1544 (1998)
124. Fritzsch H. *Phys. Lett.* B415:83 (1997)
125. Hou W-S, Tseng B. *Phys. Rev. Lett.* 80:434 (1998)
126. Yuan F, Chao K-T. *Phys. Rev.* D56:R2495 (1997)
127. Miller D, et al. (CLEO Collaboration). Report No. CLNS 94/1277 (1994); Stone S (CLEO Collaboration). *Nucl. Instrum. Meth.* A368:68 (1995)
128. Boutigny D, et al. (BaBar Collaboration). BaBar Technical Design Report, Report No. SLAC-R-95-457 (1995); Harrison PF (BaBar Collaboration). *Nucl. Instrum. Meth.* A368:81 (1995)
129. Cheng MT, et al. (Belle Collaboration). Belle Letter of Intent, Report No. KEK 94-2 (April 1994); Haba J (Belle Collaboration). *Nucl. Instrum. Meth.* A368:74 (1995)
130. Dugan G, Mikhailichenko A, Rogers J, Rubin D. "Dual Aperture Luminosity Collider at Cornell University" presented at 1997 PAC meeting at Cornell University.
131. Bordalo P, et al. (NA10 Collaboration). *Z. Phys.* C39:7 (1988); Catanesi MG, et al. (WA78 Collaboration). *Phys. Lett.* B231:328 (1989); Kodama K, et al. (E653 Collaboration). *Phys. Lett.* B305:359 (1993); Jesik R, et al. (E672/E706 Collaboration). *Phys. Rev. Lett.* 74:495 (1995); Schub MH, et al. (E789 Collaboration). *Phys. Rev.* D52:1307 (1995), Erratum *Phys. Rev.* D53:570 (1996)
132. Hartouni E, et al. (HERA-B Collaboration). Report No. DESY-PRD 95/01 (1995); Ehret K. *Proc. IInd International Conference on B Physics and CP Violation*, Honolulu, Hawaii, pp.40-47 (1997)
133. Blair R, et al. (CDF II Collaboration). CDF-II Technical Design Report, Report No. FERMILAB-Pub-96/390-E (1996)
134. Maciel AKA. *Proc. IInd International Conference on B Physics and CP Violation*, Honolulu, Hawaii, pp.27-39 (1997)
135. Abachi S (D0 Collaboration). Report No. FERMILAB-Pub-96/357-E (1996)
136. ATLAS Collaboration. ATLAS Technical Proposal, Report No. CERN/LHCC/94-43, LHCC/P2 (1994); Eerola P (ATLAS Collaboration) *Nucl. Instrum. Meth.* A384:93 (1996)
137. CMS Collaboration. CMS Technical Proposal, Report No. CERN/LHCC 94-38, LHCC/P1 (1994); Kotlinski D, et al. (CMS Collaboration) *Nucl. Instrum. Meth.* A368:115 (1995)
138. Santoro A, et al. (BTeV Collaboration). BTeV Expression of Interest, Report No. BTeV-pub-97/2 (1997); Stone S. *Proc. IInd International Conference on B Physics and CP Violation*, Honolulu, Hawaii, pp.61-73 (1997)
139. LHC-B Collaboration. Report No. CERN/LHCC 95-5, LHCC/18 (Aug 1995); Cox B. *Proc. IInd International Conference on B Physics and CP Violation*, Honolulu, Hawaii, pp.48-60 (1997)